Project Information	
Project full title	EuroSea: Improving and Integrating European Ocean Observing and Forecasting Systems for Sustainable use of the Oceans
Project acronym	**EuroSea**
Grant agreement number	862626
Project start date and duration	1 November 2019, 50 months
Project website	https://www.eurosea.eu

Deliverable information	
Deliverable number	D5.3
Deliverable title	**CMEMS downscaled circulation operational forecast system**
Description	This document describes the numerical modelling work done in task 5.2 needed to implement OSPAC.
Work Package number	5
Work Package title	Coastal Resilience and Operational Services Demonstrator
Lead beneficiary	CMCC
Lead authors	Ivan Federico (CMCC), Giovanni Coppini (CMCC), Salvatore Causio (CMCC), Maria Liste (UPC), Marc Mestres (UPC), Manuel Espino (UPC), Agustín S.-Arcilla (UPC), Marcos Garcia Sotillo (EPPE)
Contributors	Begoña Pérez Gómez (EPPE), José María García Valdecasas (EPPE), Susana Pérez Rubio (EPPE), Enrique Alvarez Fanjul (EPPE), Manuel Garcia Leon (EPPE, UPC, Nologin)
Due date	31 October 2021
Submission date	29 October 2021
Resubmission date	18 August 2023 (revised version)
Comments	

This project has received funding from the European Union's Horizon 2020 research and innovation programme under grant agreement No. 862626.

https://doi.org/10.3289/eurosea_d5.3

Table of contents

Executive summary 1
1. Introduction 1
2. Areas of Interest 2
    2.1. Taranto 2
    2.2. Barcelona 4
3. Methodology 5
    3.1. Numerical models 5
        Taranto 5
        Barcelona 5
    3.2. Bathymetry and grid generation 6
        Taranto 6
        Barcelona 7
    3.3. Boundary conditions 7
        Taranto 7
        Barcelona 10
    3.4. Physical and numerical setting 11
        Taranto 11
        Barcelona 11
4. Results 12
        Taranto 12
        Barcelona 21
5. Operational Forecasting Chains 22
6. Conclusions 24
7. References 24
    7.1. Taranto 24
    7.2. Barcelona 27

Executive summary

This document explains in detail the set-up and implementation of two numerical high-resolution models for the test cases of Taranto and Barcelona, as expected in the EuroSea workplan. Both models are state of the art and have been carefully validated. The operating services resulting will be in the core of OSPAC product, the main deliverable of WP5.2.

The third pilot involved in the project, Alexandría, does not have models ready, since this port, quite unexpectedly, failed to obtain the internally required permits to work in the project. Nevertheless, this is not a concerning delay, since all methodologies are developed, and we are already working on the modelling work for the substitute port designated (Buenaventura, in Colombia). At this moment, locations in Colombia or Madagascar are being studied. Contacts with local authorities are established and a final decision will be made before the end of 2021.

1. Introduction

The ocean is an essential part of the planet that plays a crucial role in the global life system and provides vital resources for humanity. Coastal zones are the most affected areas by direct anthropic pressures, and their management is very complex due to the multiple interconnected processes that occur there. Therefore, understanding the physical behavior of coastal zones is vital to managing the main problems related to impacts and resource exploitation activities (Liste et al., 2021). In this coastal setting, ports and adjacent cities are one of the main anthropic infrastructures that generate economic wealth. The increase in maritime traffic has resulted in rapid growth in port activity. As ports and cities are affected by met-ocean conditions, especially extreme events, personalized real-time and forecast information on environmental conditions is needed to manage their growth. Wind, waves, and sea level are traditionally the most critical met-ocean parameters.

Supporting port and city activities require accurate ocean forecasting systems. In response to this growing demand for continuous and updated met-ocean information, high-resolution models are being implemented in coastal areas, combined with in situ observations, that allow for a better understanding and characterization of the main hydrodynamic characteristics of these areas. As a result, the operational physical oceanography is maturing quickly, and ocean modelling circulation as an operational capability is now a fact.

In the framework of the EuroSea Project, the WP5 team has been working on developing a 3D hydrodynamic operational tool with enough resolution to solve the dynamics of restricted domains such as Barcelona´s and Taranto´s local coastal waters, harbors, and beaches. This deliverable provides a complete description of the CMEMS downscaled circulation operational forecast systems in Barcelona´s and Taranto´s local coastal waters.

The report is organized as follows: Section 2 describes the study site. Section 3 describes the 3D modeling systems and setups. Finally, section 4 presents validations and results.

2. Areas of Interest

2.1. Taranto

The area of interest is focused on the Southern Adriatic and Northern Ionian seas of Mediterranean basin, with special zoom in the Gulf of Taranto (hereafter GT) and particularly in the Mar Grande and Mar Piccolo where the port of Taranto is located.

The southern Adriatic Sea extends approximately southward along the latitude of 42°N to the threshold of the Strait of Otranto and has a maximum depth of 1270 m. An exchange of waters with the Ionian Sea occurs at the Strait of Otranto at approximately 40°N. The northern Ionian Sea extends south of 38°N and has a steeper continental slope than the Adriatic basin. The offshore maximum depth is 3500–3700 m.

The GT (Figure 1a) is situated in the northwestern Ionian Sea and is approximately delimited in open sea by the line connecting Apulia and Calabria (Gulf of Taranto – Boundary Section, GT-BS in Figure 1a). It is a deep, semi-enclosed ocean area in southern Italy encircled by two peninsulas, Apulia and Basilicata/Calabria (Figure 1a). It is open to the northern Ionian Sea, and a deep trench of more than 2000 m connects it to the eastern Mediterranean Sea. The continental shelf area, considered as the area from the coasts to the 200 m depth contour, occupies only 10 % of the total Gulf area (Pinardi et al., 2016) with the shelf wider on the Apulia than the Calabria side.

A complex water mass circulation (Sellschopp and Álvarez, 2003) with high seasonal variability (Milligan and Cattaneo, 2007) characterizes the GT basin. Oceanographic studies (Poulain, 2001; Bignami et al., 2007; Turchetto et al., 2007; Grauel and Bernasconi, 2010; Oddo and Guarnieri, 2011) describe two main GT surface circulation structures: (i) a cyclonic gyre encompassing the Western Adriatic Coastal Current (WACC) flowing around Apulia into the GT from the northern Adriatic Sea, and (ii) an anticyclonic circulation connected to the Ionian Surface Waters (ISW) flow entering from the central Ionian Sea. In addition, studies on the coastal current in the inner part of the GT (De Serio and Mossa, 2015) show a coastal flow supporting the anticyclonic gyre structure.

Other studies in the GT based on observations (Pinardi et al., 2016) showed that in the Gulf (i) a mixed layer thickness extending down to 30m; (ii) an intermediate water salinity maximum - indicative of Modified Levantine Intermediate Waters - in the deep part of the Gulf; and (iii) low salinity values at the surface indicating surface waters of Adriatic or Atlantic origin. Federico et al. (2017) simulated the basin-scale circulation of the GT showing the circulation structure affected by the WACC position and strength (Artegiani et al., 1997a; Artegiani et al. 1997b; Cushman-Roisin et al., 2001; Ciancia et al., 2018). The WACC normally flows southwestward out of the Adriatic Sea, entering the GT from the surface down to 100m. In some cases the WACC could be weak and a reversed northeastward coastal current could be present in Gulf along the Apulia coasts, exiting the GT-BS. On the basis of a long-term modelling reanalysis, Pinardi et al. (2016) hint on a possible reversal of the large-scale anticyclonic gyre of the GT, connecting this feature to the inflow-outflow system of the GT-BS.

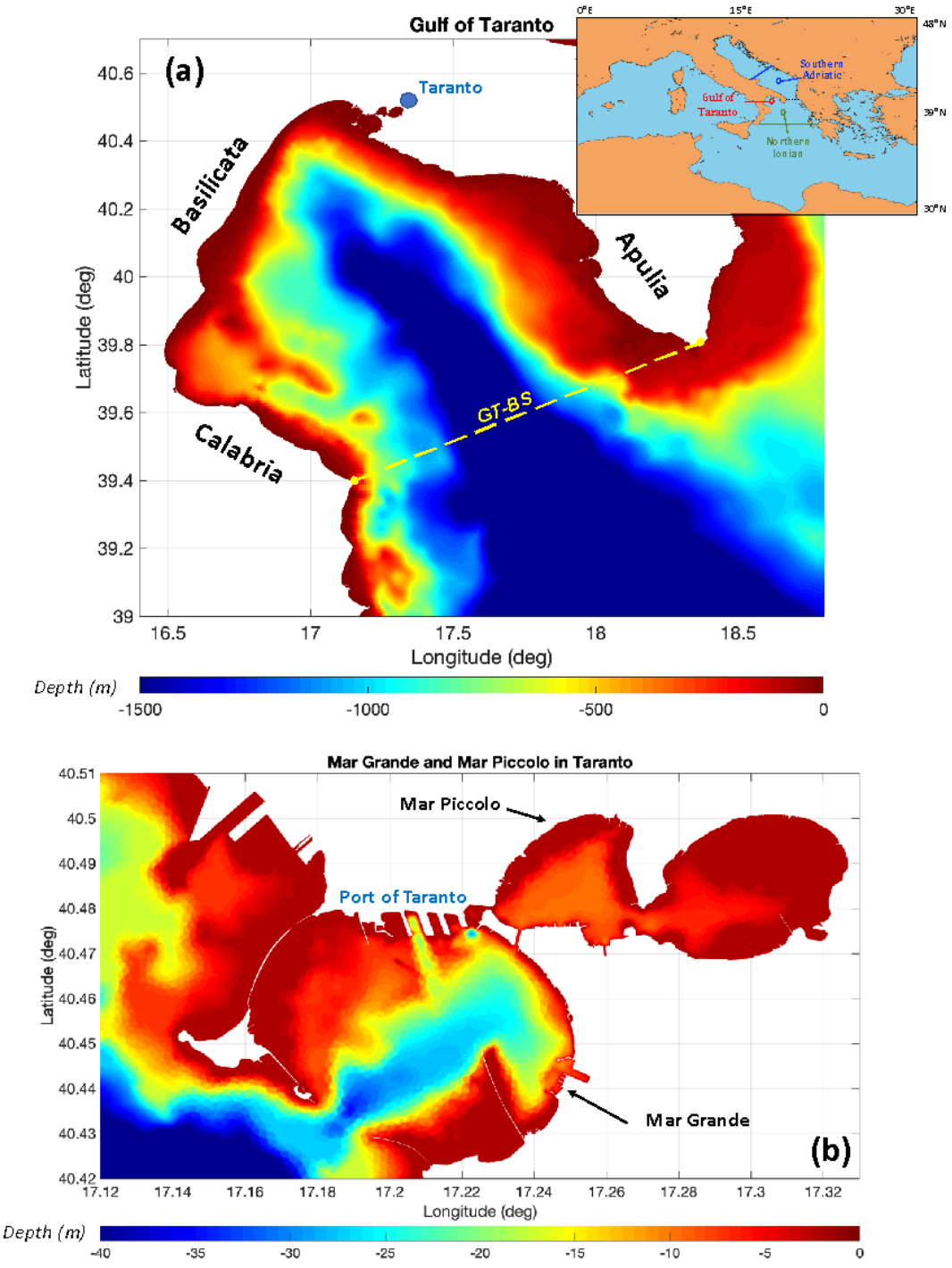

Figure 1. Area of interest: bathymetry and coastline of Gulf of Taranto (a) and Mar Grande (southwestern part of domain, where port of Taranto is located) and Mar Piccolo (northeastern part of domain) of Taranto (b)

A 7.5 km wide sheltered elliptical embayment, called the Mar Grande – Mar Piccolo system of Taranto (Figure 1b), hereafter named MG-MP, opens in the northeastern part of the GT. The MG-MP is a marine system that experienced over the last few decades strong biochemical pollution and environmental degradation, and it is considered a hotspot study site for economic, ecological and scientific reasons. In the MG-MP the circulation consists of along-shore currents, which follow the direction of the wind and are modulated by

tidal forcing (Scroccaro et al., 2004) with a tidal range of about 20 cm (Umgiesser et al., 2014). In Umgiesser et al. (2014) and Ferrarin et al. (2014), a 3D, annual and baroclinic model simulation of the Taranto basin was performed, focusing on mixing capacity and comparison with other Mediterranean lagoons. De Pascalis et al. (2016) described the averaged fields of MG-MP, showing that the basin is dominated by estuarine dynamics, but it could be that the Gulf would switch between the two opposite vertical circulations during the year (Federico et al., 2017).

2.2. Barcelona

In particular, the study area is focused on the coastal waters and port of Barcelona city, located on the Catalan coast in the Northwest Mediterranean Sea (see Figure 2). It corresponds to the northern section of the Spanish coast, situated between latitudes 40°45' N and 42°25' N and longitudes 0°45' E and 3°15' E, with an extension of around 700 km (Pallares et al. 2014).

Orographic patterns, air-sea temperature differences and the passage of low-pressure centres from the Atlantic mainly control the meteorological situation in the area. The Pyrenees, situated north of the Catalan coast, act as a physical barrier that modifies the wind patterns and produces the Mistral and the Tramontana, northwest, and north winds, respectively, whose influence can be noticed hundreds of kilometres offshore (Bolaños et al., 2009). Also, the wind channelling due to river valleys and the complex topography generate highly variable wind patterns in space and time.

The prevalent winds come from the north and northwest, primarily during December and January; southerly and easterly winds are also significant, particularly during February, March, April and November (Arnau, 2000). On average, the winds are not very intense. The maximum velocities correspond to easterly winds in agreement with storm conditions. ; the most energetic storms registered in the area are associated with this directional sector and affect the entire length of the Catalan coast (Mendoza et al., 2011).

The general circulation pattern presents a relatively complex pattern primarily determined by the bottom bathymetry (Sánchez-Arcilla and Simpson, 2002). The characteristics of the continental shelf and the slope are crucial: in the north, the shelf is broad (about 70 km), narrows to less than 20 km in the central stretch of the coast (in front of Barcelona city), and then widens again abruptly to about 60 km further south. Due to the microtidal character of the Mediterranean Sea, tidal perturbations to the currents are not significant in this area (Poulain et al., 2013; Tsimplis et al., 1995).

The predominant wave directions, as with the wind, vary along the coast clearly showing the topographic control due to a complex bathymetry, with submarine canyons and a heterogeneous continental shelf width (Sánchez-Arcilla et al., 2008; Bolaños et al., 2009). Sánchez- Arcilla et al. (2008) describe how waves from east and south are the prevailing wave conditions in the study area. The largest waves come from the east, where the largest fetches and stronger winds coincide (Pallares et al. 2014).

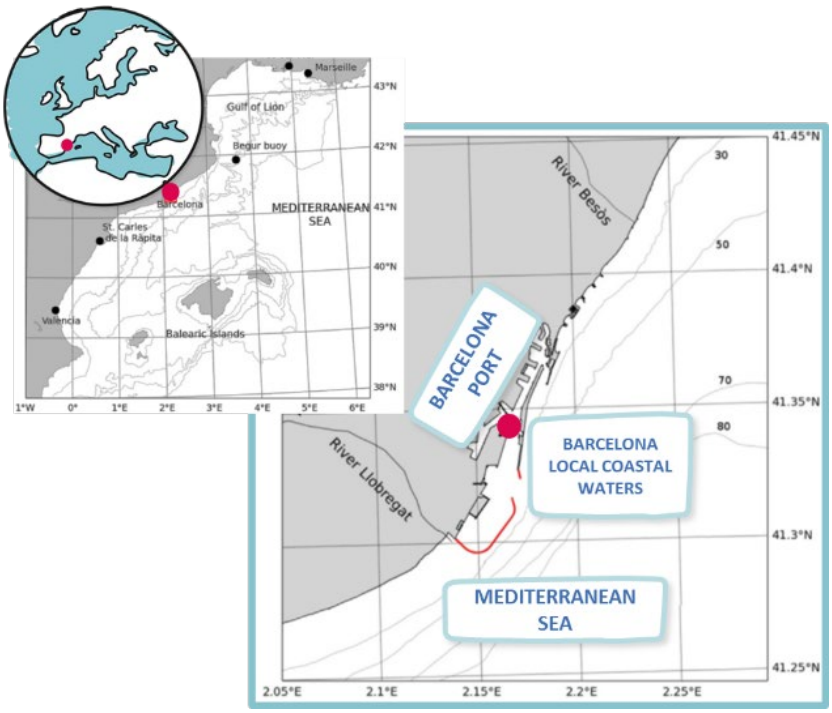

Figure 2. (Left corner) Extended study area comprising the NW Mediterranean. Focus is placed around the Barcelona local coastal waters and port area. Isobaths are drawn up to 80m.

3. Methodology

3.1. Numerical models

Taranto

The modelling system is based on the SHYFEM model, which is a 3-D finite element hydrodynamic model (Umgiesser et al., 2004) solving the Navier–Stokes equations by applying hydrostatic and Boussinesq approximations. The unstructured grid is Arakawa B with triangular meshes (Bellafiore and Umgiesser, 2010; Ferrarin et al., 2013), which provides an accurate description of irregular coastal boundaries. The scalars are computed at grid nodes, whereas velocity vectors are calculated at the center of each element. Vertically a z layer discretization is applied and most variables are computed in the center of each layer, whereas stress terms and vertical velocities are solved at the layer interfaces (Bellafiore and Umgiesser, 2010). The peculiarity of unstructured meshes is the ability of representing several scales in a seamless fashion, reaching higher resolution where necessary.

The model uses a semi-implicit algorithm for integration over time, which has the advantage of being unconditionally stable with respect to gravity waves, bottom friction and Coriolis terms, and allows transport variables to be solved explicitly. The Coriolis term and pressure gradient in the momentum equation, and the divergence terms in the continuity equation are treated semi-implicitly. Bottom friction and vertical eddy viscosity are treated fully implicitly for stability reasons, while the remaining terms (advective and horizontal diffusion terms in the momentum equation) are treated explicitly. A more detailed description of the model equations and of the discretization method is given in Umgiesser et al. (2004) and Ferrarin et al. (2017).

The model has been already applied to simulate hydrodynamics of several systems in many regions of world, proving its quality and accuracy. Exploiting the variable mesh approach, the model has been successfully applied to several scales, from the open sea (e.g., Mediterranean Sea, Black Sea, Gulf of Mexico) to the coastal seas and estuaries (e.g., coastal areas of Adriatic Ionian and Western Mediterranean Seas in Italy, Kotor Bay in Montenegro, Danube Delta in Romania) to open-sea islands (e.g., Malta) to the fjords (e.g., Roskilde, Denmark, Oslo) to the lagoons (e.g., Venice, Menor in Spain, Nador in Morocco, Dalyan in Turkey, Curonian in Lithuania, Tam Giang in Vietnam) to the ports (e.g., Apulian ports in Italy) to the rivers (e.g., Po river in Italy, Savannah river in Georgia, US) to the lakes (e.g., Geneva in Switzerland, Garda in Italy).

The modelling approach is based on the downscaling of CMEMS Marine products released at the regional scale of Mediterranean Sea. The current Med-CMEMS implementation is based on NEMO (Nucleus for European Modelling of the Ocean; Madec, 2008) finite-difference code with a horizontal resolution of 1/24 of a degree (4–5 km approximately) and 141 unevenly spaced vertical levels. The system is provided by a data assimilation system based on the 3D-VAR scheme developed by Dobricic and Pinardi (2008).

Barcelona

The 3D hydrodynamic tools described in this deliverable are based on the COAWST Modelling System (Warner et al., 2010), a three-dimensional hydrodynamic model integrating atmosphere and ocean circulation, surface waves, and sediment transport components.

COAWST framework system is used to develop two ocean circulation model configurations. The first one, called OSPAC V1, is now operational using the ocean circulation model and fields. The second one, called OSPAC V2, is now ready to be implemented in operational but, for now, is only running offline using the coupling circulation and waves models and fields. Based on the Model Coupling Toolkit, COAWST enables the exchange of information among numerical models representing different processes of the oceanic system, thus allowing an explicit description of their interactions. We used the latest available version of the COAWST modelling system (version 3.7), as of the date of publication of this deliverable. However, complete model details are available on the COAWST website[1] for detailed checks and future improvements.

Both model configurations are described in detail below:

<u>OSPAC V1:</u>

In the OSPAC V1 configuration, high-resolution simulations have been performed by circulation fields using the Regional Ocean Modelling System (ROMS Model). ROMS is a three-dimensional, free-surface, topography-following numerical model that solves finite difference approximations of Reynolds Averaged Navier Stokes (RANS) equations using hydrostatic and Boussinesq approximations with a split-explicit time-stepping algorithm (Shchepetkin and McWilliams, 2005; Haidvogel et al., 2008; Shchepetkin and McWilliams, 2009). In addition, ROMS includes options for various model components such as different advection schemes (second, third, and fourth-order), turbulence closure models (e.g., Generic Length Scale mixing, Mellor-Yamada, Brunt-Väisälä frequency mixing, user-provided analytical expressions, K-profile parameterization), and several options for boundary conditions.

[1] https://www.usgs.gov/software/coupled-ocean-atmosphere-wave-sediment-transport-coawst-modeling-system

OSPAC V1 used the latest available version of the ROMS model (version 3.9) as of the date of publication of this deliverable. However, numerical details and a complete model description, user documentation, and source code are available at the ROMS website[2] for future checks and improvements.

OSPAC V2:

In the OSPAC V2 configuration, high-resolution simulations have been performed by coupling circulation and waves fields, ocean circulation using the ROMS Model (described above), and surface waves using the Simulating Waves Nearshore Model (SWAN Model). SWAN is a spectral wave model that solves the transport of wave action density and includes source terms from wind and sinks terms to include wave energy dissipation due to white capping, breaking, and bottom friction (Booij et al., 1999). The simulations are based on a two-way coupling between ROMS and SWAN running on the same computational grid.

OSPAC V2 used the latest available versions of the ROMS model (version 3.9) and the SWAN Model (version 41.31) as of the date of publication of this deliverable. However, all model details are available at the ROMS website[2] and SWAN website[3] for future checks and improvements.

3.2. Bathymetry and grid generation

Taranto

Starting from the experience of the first implementation of the Southern Adriatic Northern Ionian coastal Forecasting System (Federico et al., 2017), here in EuroSea we have developed a specific and iper-resolution configuration for Taranto Seas. The new system covers only the GT with a horizontal resolution from 3km in open-sea to 100m in the coastal waters to 20m in the port of Taranto. Figure 3 shows the grid and bathymetry in GT and MG-MP. A single open boundary is created connecting Calabria and Apulia coasts through the GT-BS (Figure 1a). This configuration has been created to perform specific process studies and long-term hindcast simulations, due to the reduced density meshes in respect with the first one. The new horizontal grid has been be created adopting advanced and customized tools (mainly python-based) of meshing based on GMSH[4] and BLENDER[5] software.

The bathymetry was derived from the EMODnet[6] product at resolution of 1/8 x 1/8 arc-minutes (circa 230 x 230 meter) resolution for open sea and coastal waters and integrated with higher-resolution bathymetry (resolutions of order of meter) for coastal areas in MG-MP and Taranto Port area provided by the Italian Navy Hydrographic Institute. The vertical discretization is based on z-layers approach. The vertical spacing is 2 m until 90 m from the sea surface, the resolution is then progressively (stepwise) increased down to the bottom with a maximum layer thickness of 200 m. This is appropriate for solving the field both in coastal and open-sea areas.

Barcelona

Bathymetries are built using a combination of bathymetric data from EMODnet[6] and specific high-resolution sources provided by Barcelona Port Authority. An updated and higher resolution bathymetry is also applied

[2] http://www.myroms.org/

[3] https://swanmodel.sourceforge.io/

[4] http://gmsh.info/

[5] https://www.blender.org/

[6] https://www.emodnet-bathymetry.eu/

to adjust the open boundary to the coastal bathymetries in the port domains. Finally, the bathymetry information interpolated at the mesh is smoothed using a Shapiro filter with an r-factor criterion below 0.25.

The bottom boundary layer was parameterized with a logarithmic profile using a characteristic bottom roughness height of 0.002 m. The turbulence closure scheme for the vertical mixing is the generic length scale (GLS) tuned to behave as k-epsilon (Warner et al., 2005). Horizontal harmonic mixing of momentum is defined with constant values of 5 m^2s^{-1}.

3.3. Boundary conditions

Taranto

The modelling system is three-dimensionally downscaled from Med-CMEMS both in terms or initialization and open boundaries. The scalar fields from Med-CMEMS (non-tidal sea surface height, temperature, and salinity) are treated at the boundary nodes of nested system through a clamped boundary condition. The velocity fields are imposed as nudged boundary condition from parent model in the barycentre of the triangular elements using a relaxation time of 3600 s. The tidal elevations derived from the OTPS (Oregon State University Tidal Prediction Software, Egbert and Erofeeva, 2002) tidal model with 1/30 horizontal resolution are added at the Med-CMEMS sea surface height and prescribed at each boundary node. Eight of the most significant constituents are considered for astronomical tidal model: M2, S2, N2, K2, K1, O1, P1, Q1.

Three basic surface boundary conditions are used:

a) For temperature, the air-sea heat flux is parameterized by bulk formulas described in Pettenuzzo et al. (2010).
b) For momentum, surface stress is computed with the wind drag coefficient according to Hellermann and Rosenstein (1983).
c) For the vertical velocity and the salinity, the salt flux boundary condition is adopted and the water flux advected through the air-sea interface is given by precipitation minus evaporation.

For the atmospheric fields, well-consolidated products from ECMWF (6.5 km resolution and 3h frequency) are adopted as forcing. The atmospheric fields are corrected by land-contaminated points following Kara et al. (2007) and horizontally interpolated at each ocean grid node by means of Cressman's interpolation technique (Cressman, 1959).

The atmospheric variables used for the parametrization are 2 m air temperature (T2M), 2 m dew point temperature (D2M), total cloud cover (TCC), mean sea level atmospheric pressure (MSL), and meridional and zonal 10 m wind components (U10M and V10M) and total precipitation (TP).

Rivers and wastewater inputs as well as submarine springs (citri) are treated as clamped boundary conditions imposing the discharge, salinity, and temperature.

In GT, five main rivers (Bradano, Basento, Agri, Sinni and Crati, as reported in Figure 3) discharge from the western coastline with a relatively low annual mean runoff (~75 m^3/s, Verri et al., 2018). Due to a lack of available observations, river inflow surface salinity is fixed to a constant value of 0.1 at the river boundaries.

In MG-MP, we implemented the fresh water sources reported in De Pascalis et al. (2016), collecting the final report of the SPICAMAR projects (2003 and 2009) as detailed in Caroppo et al. (2011). The submarine springs have been introduced in the modelling system in terms of discharge starting from the dataset reported in De Pascalis et al. (2016), collecting the studies of Stefanon and Cotecchia (1969), Scroccaro et al. (2004), Cerruti

(1948), Spizzico and Tinelli (1986). The salinity values reported by the authors were around 5 psu due to the water seepage through the underwater karst rocks.

Water temperature at the river, freshwater and spring source boundaries adapt to the environmental inner value inside the basin.

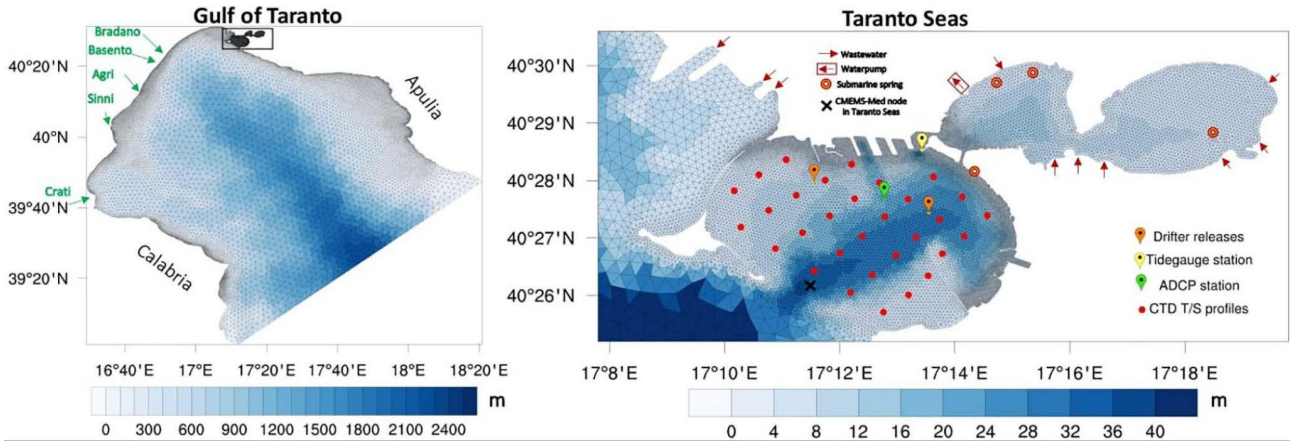

Figure 3. (a) Horizontal grid with bathymetry overlapped for Gulf of Taranto system; green arrows indicate rivers discharging in Gulf of Taranto. (b) Horizontal grid with bathymetry overlapped in the MG-MP. Symbols indicate wastewater discharge, waterpump and and submarine springs (as reported in De Pascalis et al., 2016), and observed data used for validation.

Barcelona

Grid refinement is used to nest down to the study zone along with the entire domain (Figure 4). Both OSPAC V1 and V2 model applications consist of 2 nested regular grids with a spatial resolution of ~350 m and ~70 m for the coastal waters (CSTBCN grid) and port domain (PRTBCN grid), respectively (see Figure 5 for examples of domains and bathymetries). The nesting ratio (~5) between coastal and port domains is defined to get enough resolution to reproduce the circulation due to the inner shape of the port considering the mesoscale dynamics of the coastal domain. The chosen vertical discretization consists of 20 sigma levels for the coastal water domain (CSTBCN grid) and 15 levels for the Barcelona port domain (PRTBCN grid).

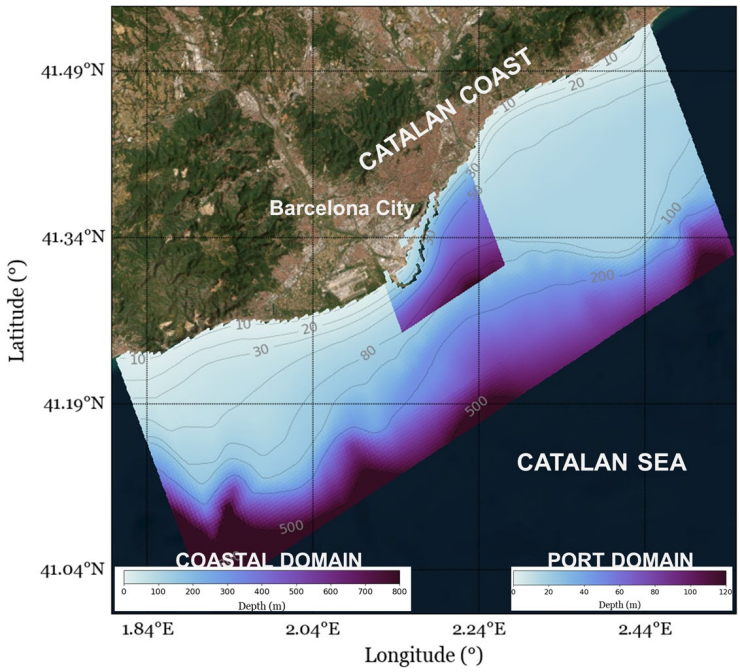

Figure 4. Horizontal grid with bathymetry overlapped for the Coastal domain and Port domain. Note that the colour scale for the bathymetry is different to visualize the Port domain grid within the Coastal domain grid.

Both OSPAC V1 and V2 models are nested into the daily updated regional ocean forecast products delivered by CMEMS- IBI (Sotillo et al., 2015). At the sea surface, the models are driven by high frequency (hourly) wind stress, atmospheric pressure, and fluxes of water and surface heat derived from the Spanish Meteorological Agency (AEMET) forecast services, based on two operational applications of the HIRLAM (High-Resolution Limited Area Model): One, the HNR (0.05° resolution and a forecast horizon of + 36 h), covering the Spanish territory and another covering the more extended regional euro-Atlantic ONR application (0.16° resolution and a forecast horizon of + 72 h). Further detailed information on this methodology can be found in Sotillo el et al. (2019).

The HNR and ONR fields are jointly used according to the best available basis and pre-processed to obtain wind surface stress, surface net heat, and salinity fluxes. Hourly barotropic water currents and sea level are provided by CMEMS-IBI and consistently applied as Open Boundary Conditions (OBC) with Chapman and Flather algorithms (Carter and Merrifield, 2007). Moreover, daily average values of CMEMS-IBI currents, temperature, and salinity are imposed through the water column as clamped (Dirichlet) boundary conditions (Sotillo et al., 2019).

3.4. Physical and numerical setting

Taranto

About the main numerical settings, we use a TVD (total variation diminishing) scheme for both the horizontal and vertical advection in the transport and diffusion equation for scalars, with constant diffusivity.

Horizontal advection of momentum is discretized by an upwind scheme and horizontal eddy viscosity is computed by the Smagorinsky's formulation.

For the computation of the vertical viscosities and diffusivities, a k–ε turbulence scheme is used, adapted from the GOTM (General Ocean Turbulence Model) model described in Burchard et al. (1999).

The bottom drag coefficient is computed using a logarithmic formulation via bottom roughness length, set homogeneous over the whole system to a value of 0.01 m (Ferrarin et al. 2017).

Barcelona

The numerical simulations are performed on two-nested grids configurations (Figure 5). OSPAC V2 is performed on two-nested grids configurations with two-way ocean refinement and one-way wave refinement with coupled exchanges between two grids for the fields of currents, bathymetry from the ocean to the wave, and wave dissipation, height, length, and direction, surface and bottom periods, and bottom orbital velocities from the wave to the ocean model (Figure 5).

Ocean model was forced with atmospheric data of winds, pressure, air temperature, relative humidity, precipitation, and heat fluxes from CMEMS-IBI. At the sea surface, the models were forced by high frequency (hourly) wind stress, atmospheric pressure, and fluxes of water and surface heat derived from the Spanish Meteorological Agency (AEMET) forecast services.

The model grids were time stepped with 60 and 15 s (for Coastal and Port grids) for the ocean, and 30 and 15 s for the wave model.

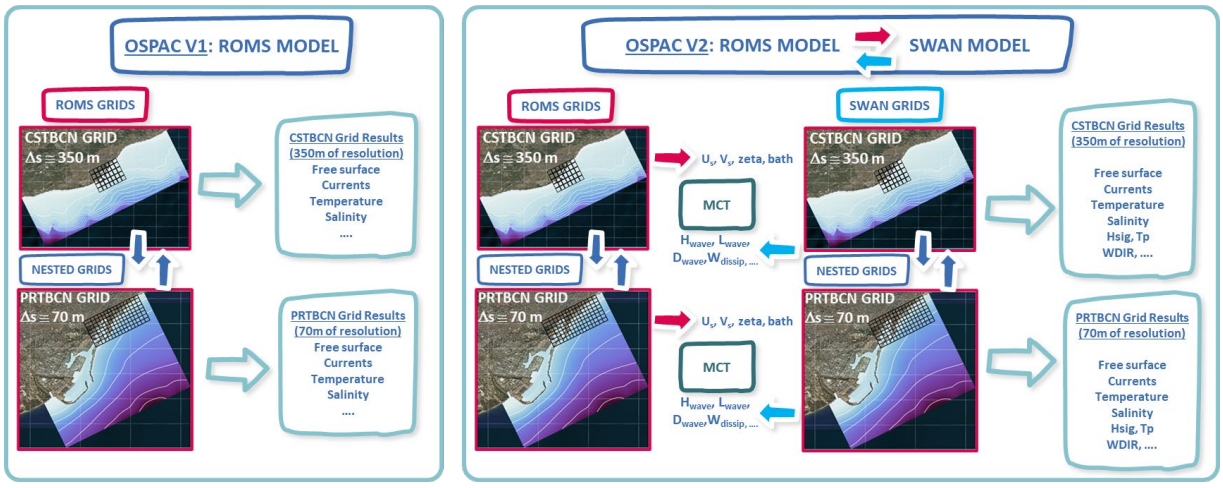

Figure 5. The left panel shows OSPAC V1 numerical configuration operational scheme. The right panel shows OSPAC V2 numerical configuration scheme.

4. Results

Taranto

The GT configuration has been run in active model for a recent period (2018-2019). One month (December 2017) of spin-up is performed. Here we show results in the coastal and harbor scale of Taranto and a quantitative analysis comparing the modelling results with observations.

Figure 6 shows surface and bottom current velocity fields, averaged over the whole year in MG-MP area. The estuarine circulation and the different behavior of the two layers is immediately clear. The surface circulation

(Figure 6a) is mainly flowing out from the Mar Piccolo to the Mar Grande and the Gulf of Taranto. The surface fresh water inputs effect is well visible because this fresh water tends to remain on the surface layer due to its low density. In general, the surface current values in the Mar Piccolo are very low, varying in a range between 0 and about 10 cm/s. The averaged bottom circulation shows a quite different trend, and Figure 6b represents the last available layer in every node of the computational grid, following the bathymetry changes. The flow moves in the opposite direction going into the Mar Piccolo basin through the narrow channels with higher mean velocities. The effects submarine springs are also clearly visible as current hotspots in Figure 6b. The velocity at the bottom of the basin is, in general, lower than the surface one.

The study on the circulation in MG-MP is qualitatively in agreement with other reference studies (e.g., De Pascalis et al., 2016).

The maps of monthly mean surface temperature of MG-MP system are reported in Figure 7. It is worth to note the difference in terms of spatial distribution between the two basins. The Mar Grande is colder than Mar Piccolo during the wintertime (highlighted for Nov, Dec, Jan, Feb), while it is warmer during the other months. The signal of submarine springs and wastewater discharges are clearly evident in some months (e.g., citrus in Mar Grande close to the port of Taranto in July, wastewater discharges in northwestern part of domain outside MG-MP).

The monthly mean surface salinity in MG-MP system (Figure 8) shows fresher fields in Mar Piccolo, with the maximum difference between the two basins in Nov and Dec. These differences could be due to (i) the presence of a larger number of fresher springs in Mar Piccolo than in Mar Grande, and (ii) the open-sea direct influence in GT in Mar Grande. Also, for the salinity fields the modelled submarine springs and wastewater are well noticeable (e.g for June 2019 as marked in Figure 8).

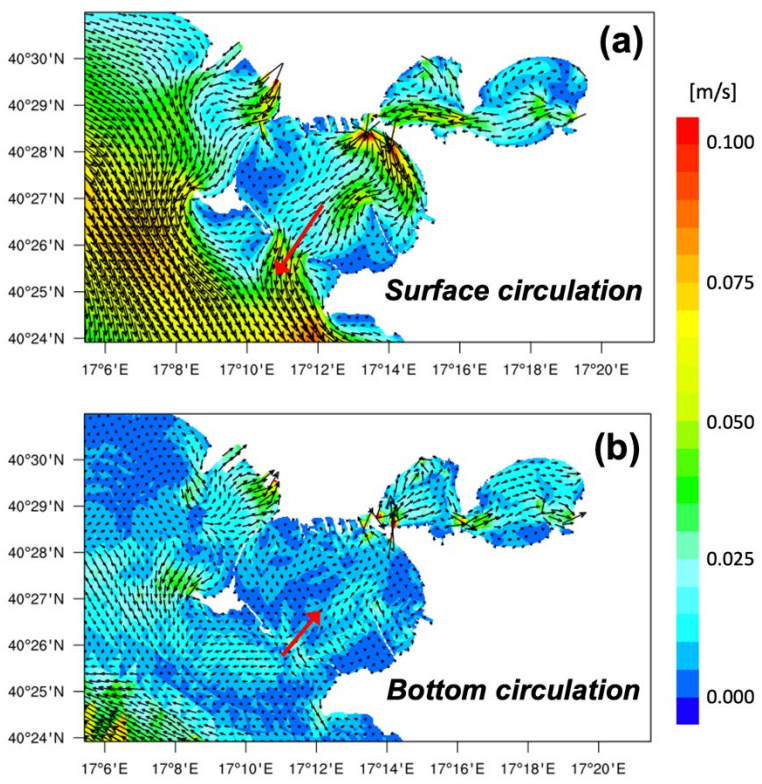

Figure 6. Yearly average (2018-2019) surface (a) and bottom (b) circulation in Mar Grande and Mar Piccolo of Taranto

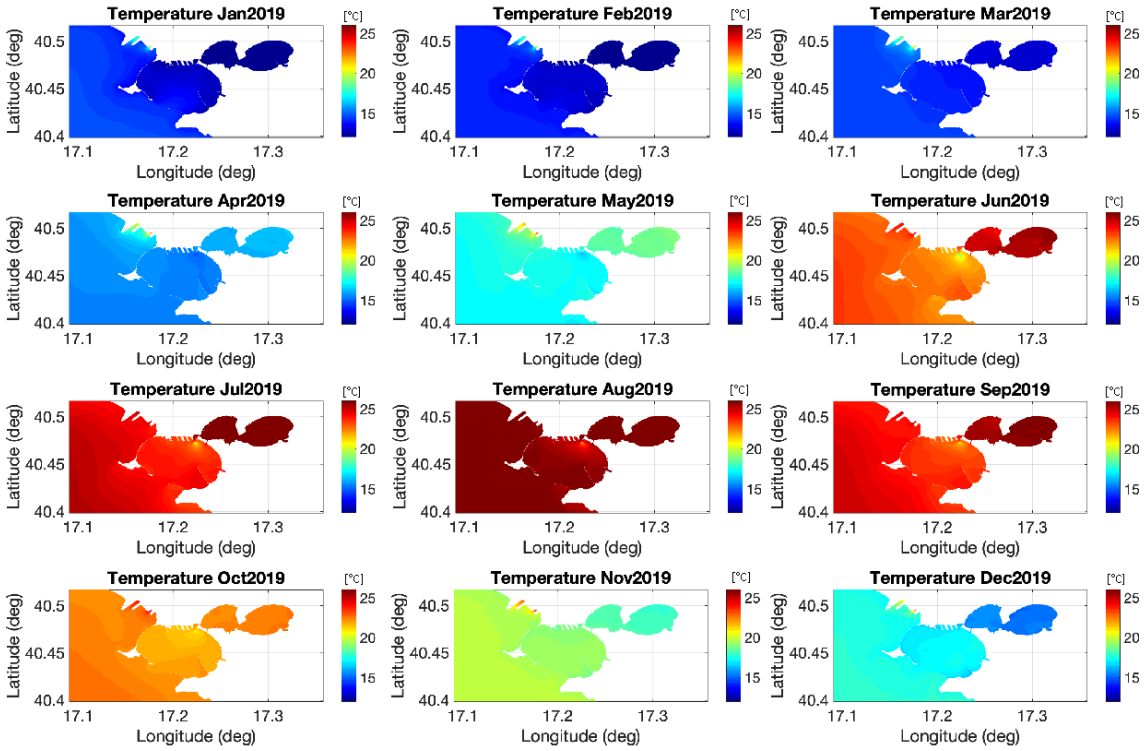

Figure 7. Monthly average (2019) surface temperature in Mar Grande and Mar Piccolo of Taranto

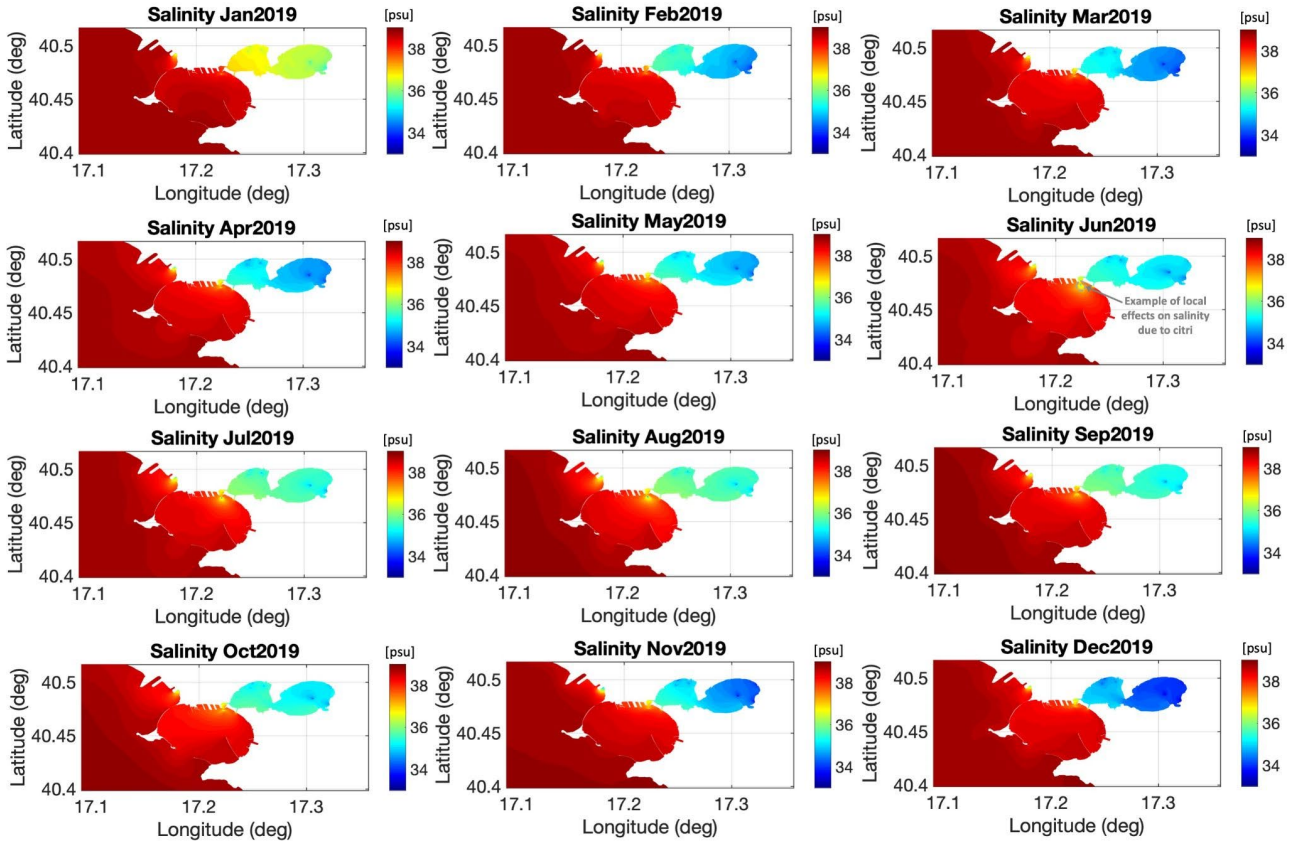

Figure 8. Monthly average (2019) surface salinity in Mar Grande and Mar Piccolo of Taranto

The modelling results have been here displayed for the tidegauges in Taranto (see Figure 3b for the location). Due to a long period of unavailability of observing data by the Taranto tidegauge (from October 2016 to March 2019), we had the opportunity to compare the model with the observations only for the period 2019/03/28 – 2019/12/31. Results of sea level comparison are reported in Figure 9, where we use daily mean outputs from model, and Figure 10, where we use hourly instantaneous outputs from model. In particular, Figure 9b highlights the BIAS between model and observations at the tidegauge station in Taranto Port. Here the GT modelling system is in satisfactory agreement with observation, with highest discrepancy in September 2019 and December 2019 (model overestimates the observations up to 10cm). The average BIAS and RMSE over the entire timeseries are 2.2 cm and 3.1 cm respectively.

Furthermore, the sea level hourly snapshots of GT model are compared in Figure 10 with tidegauge in Taranto Port, also in terms of BIAS, for different periods: 2019/03/28 – 2019/06/05 (Figure 10a), 2019/06/05 – 2019/08/13 (Figure 10b), 2019/08/13 – 2019/10/22 (Figure 10c), 2019/10/23 – 20191231 (Figure 10d). The model is qualitatively in satisfactory agreement with observation in terms of phase and with a general underestimation of amplitude. The highest differences are reported for the period 2019/09/10-2019/09/20 (Figure 10c), during the extreme event impacting Taranto on 2019/11/12 (Figure 10d) with an underestimation of 15cm by the model, and for the days of 2019/12/11-12 with model overestimation.

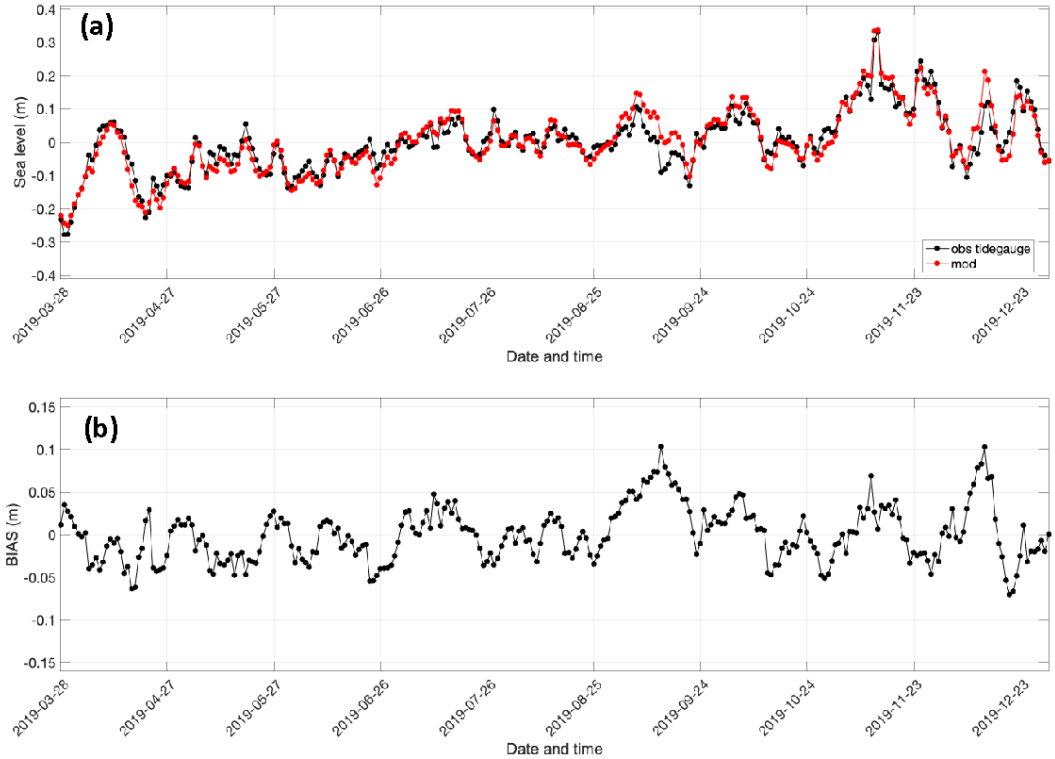

Figure 9. Sea level (daily mean) comparison of GT model with tidegauge in Taranto Port (a) and BIAS of model vs. observations (b)

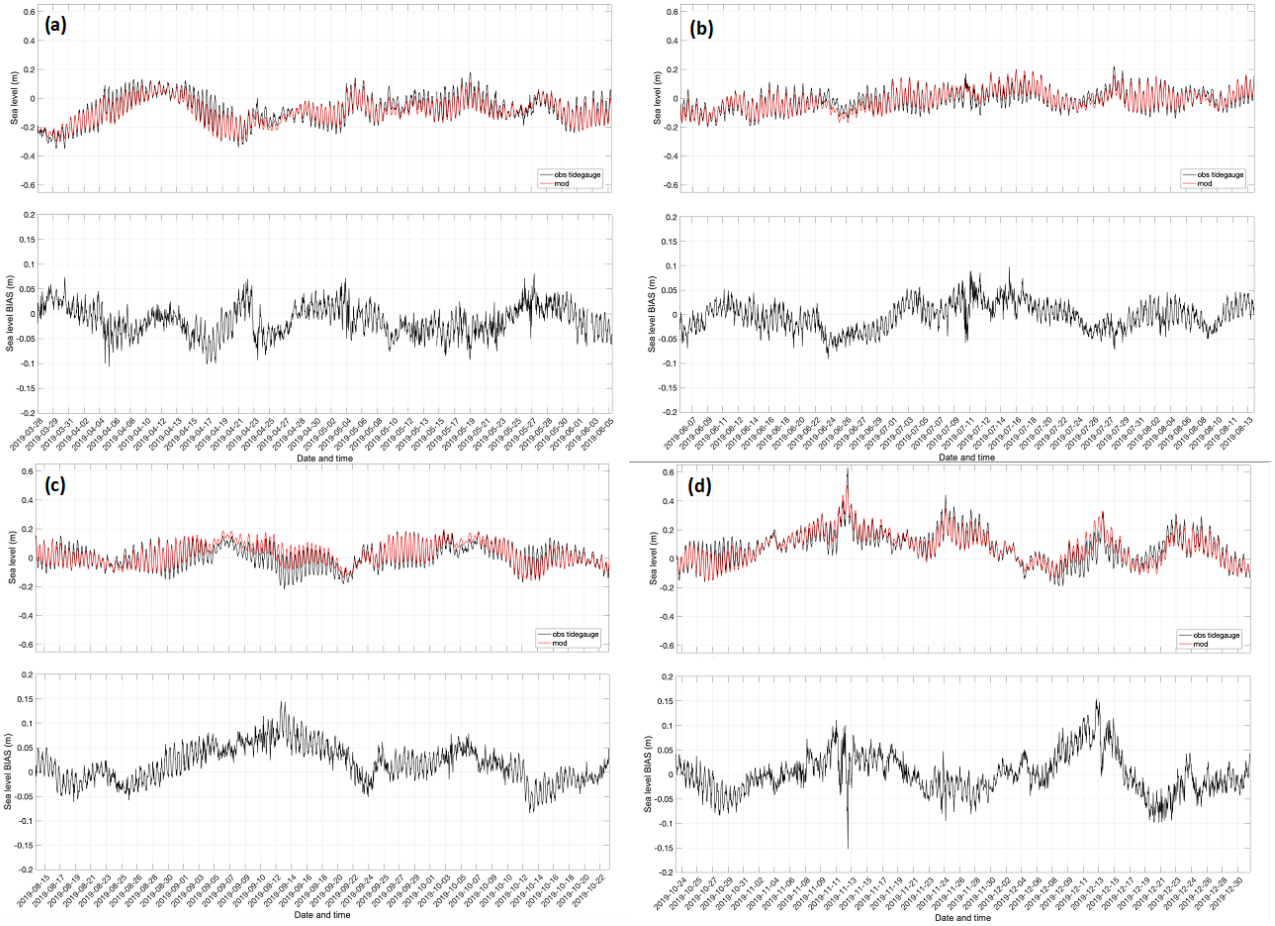

Figure 10. Sea level (hourly snapshot) comparison of GT model (red line) with tidegauge (black line) in Taranto Port for different periods (upper panels) and BIAS (lower panels): (a) 2019/03/28 – 2019/06/05, (b) 2019/06/05 – 2019/08/13, (c) 2019/08/13 – 2019/10/22, (d) 2019/10/23 – 20191231.

Here follow the main outcomes of the sea surface temperature validation. The GT simulation carried out in active model for the period 2018-2019 (with one month - December 2017 - of spin-up) has been analyzed to assess the accuracy of the model in comparison with satellite temperature. In particular, the temperature field at surface layer of model has been compared with CMEMS observation product: Mediterranean Sea Ultra High Resolution (0.01°) Sea Surface Temperature Analysis (SST_MED_SST_L4_NRT_OBSERVATIONS_010_004, Buongiorno Nardelli et al., 2013). The comparison refers to the instantaneous value at 00:00 of the model surface temperature against the satellite foundation SST (~ SST at midnight). Figure 11 shows the time series (January 2018-December 2019) of daily SST BIAS and RMSE, between model and satellite observation, averaged over the whole Gulf of Taranto domain (see Figure 3a). The model is in well agreement with the observation, describing the pattern of seasonal cycle of temperature (Figure 11a). BIAS and RMSE time series are displayed in Figure 11b and Figure 11c respectively, showing a mean (over the entire domain and entire timeseries 2018-2019) BIAS of 0.17C and a RMSE of 0.64C. The larger discrepancy between model and observations are reported in April-May 2018, May-June 2019 and August-September 2019.

The GT system was adopted also to run a short-term period (1-11 October 2014, +5 days of spin-up) which we have the availability of different observing dataset (ADCP and CTD) collected during an oceanographic survey named MREA14 and described in Pinardi et al. (2016). The velocity fields of GT have been compared

with the observed ADCP data recorded at the surface (see the location in Figure 2) and with the CMEMS-Med model in Figure 12. The comparison shows a remarkable similarity between the GT model fields and the observations, which is evident in the tidal cycle affecting the circulation and on the directions. The results demonstrate that the GT model is capable of propagating the tidal signal from the lateral open boundary condition to inshore.

Figure 13 shows the mean trajectories of two groups of drifters released in the positions (yellow dots in Figure 3b), for the first 12 h after their release (5 October 2014). The observed trajectory is shown in black and is compared to those simulated by the Lagrangian model using the GT model and CMEMS model data. The CMEMS data are derived from the single grid point outside the Taranto Sea (black cross on the right panel of Figure 3b), chosen ad hoc for the simulation. For the eastern group of drifters, the GT model trajectory shows a significant improvement, while for the western group the GT model and CMEMS drifts are equivalent. This could be due to limitations in our modelling hypothesis, such as the low spatial/temporal variability of wind forcing and the neglected effects of Stokes drift. However, the inherent limited predictability of objects floating at sea can only be ameliorated by ensemble methods.

Figure 14 shows the model comparison between GT model and CMEMS and the temperature CTD data collected during the MREA14 survey. The spatial distribution of the CTD profiles (red circles on Figure 3b) is very dense (spacing between the stations is less than 1 km), due to the need to sample the coastal and local scale features. The 31 CTD temperature casts have been averaged to produce a representative profile of the Taranto Sea, as reported in the left panel of Figure 14, together with the modelled profiles. GT model is close to the observed temperature profile, showing a significant improvement in terms of the coarse resolution CMEMS analyses, as represented by a single grid point located near the entrance of the Taranto Sea (black cross in Figure 3b). The improvement is evident in the BIAS profile (Figure 14, center panel), which is 0.13°C for GT model and is 0.3°C for CMEMS. For the RMSE profile (Figure 14, right panel) values of 0.15°C and 0.32°C are obtained for GT model and CMEMS, respectively.

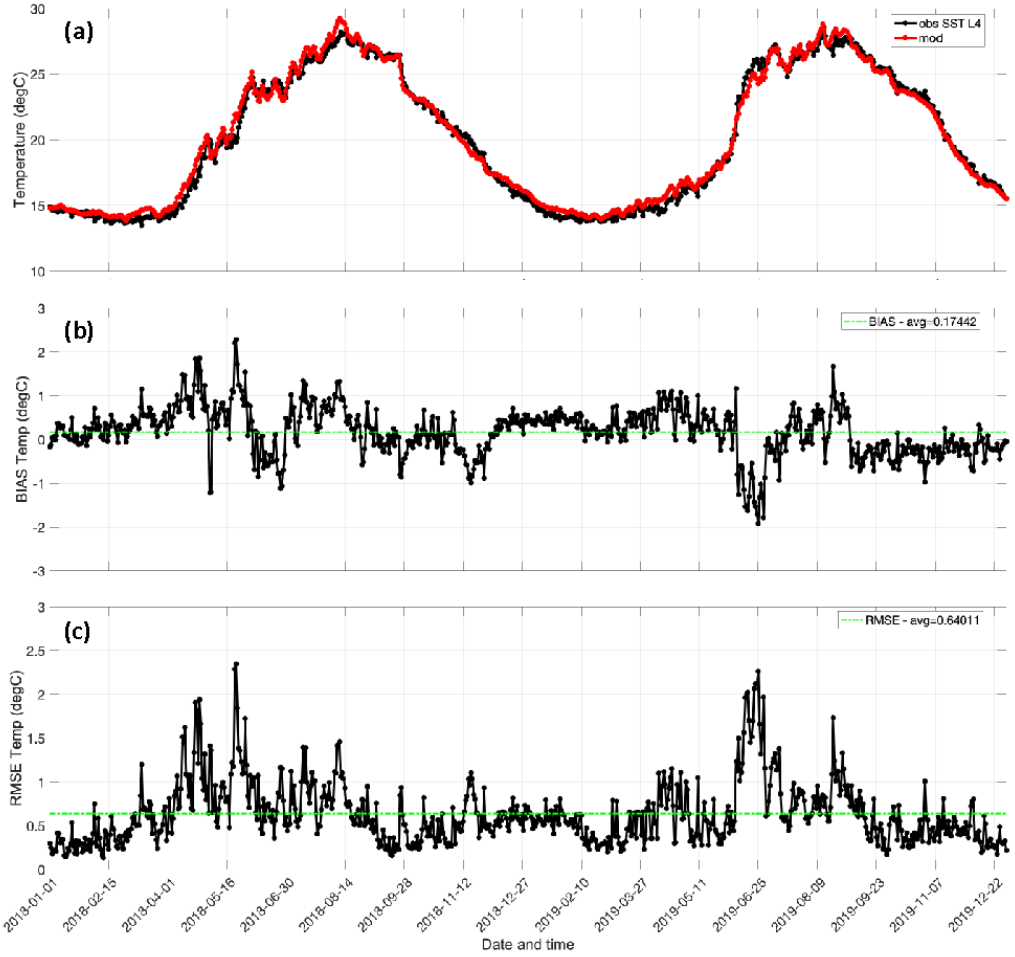

Figure 11. Time-series comparison between model surface temperature (instantaneous value at 00:00) and satellite foundation SST (~ SST at midnight), averaged over the Gulf of Taranto basin (a); BIAS (b) and RMSE (c) between model and observation (CMEMS Observation products: SST_MED_SST_L4_NRT_OBSERVATIONS_010_004).

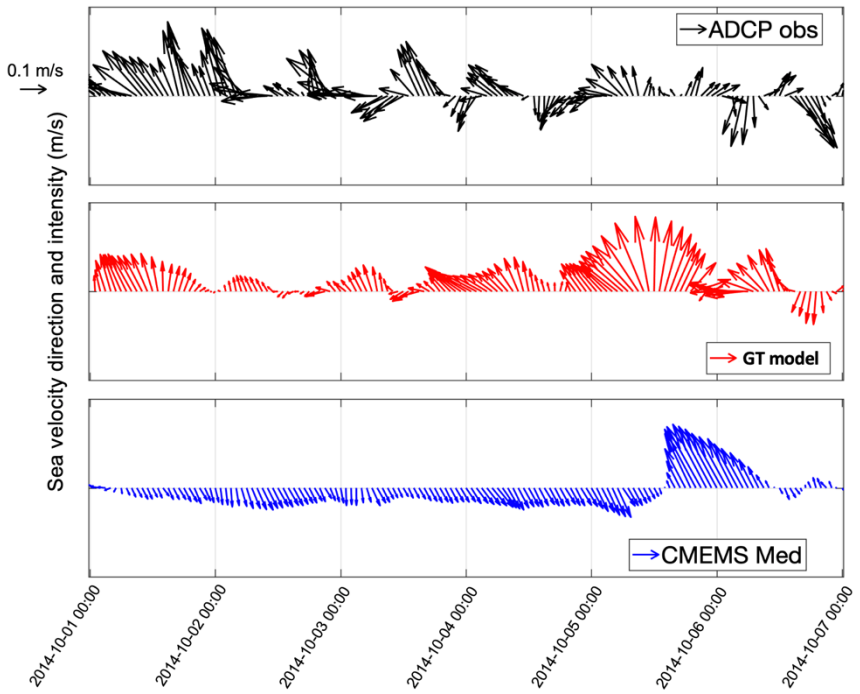

Figure 12. Time series of sea velocity direction and intensity, as measured by ADCP (black rows) and modeled by GT model (red rows) and by CMEMS Med (blue rows) (bottom panel) are given.

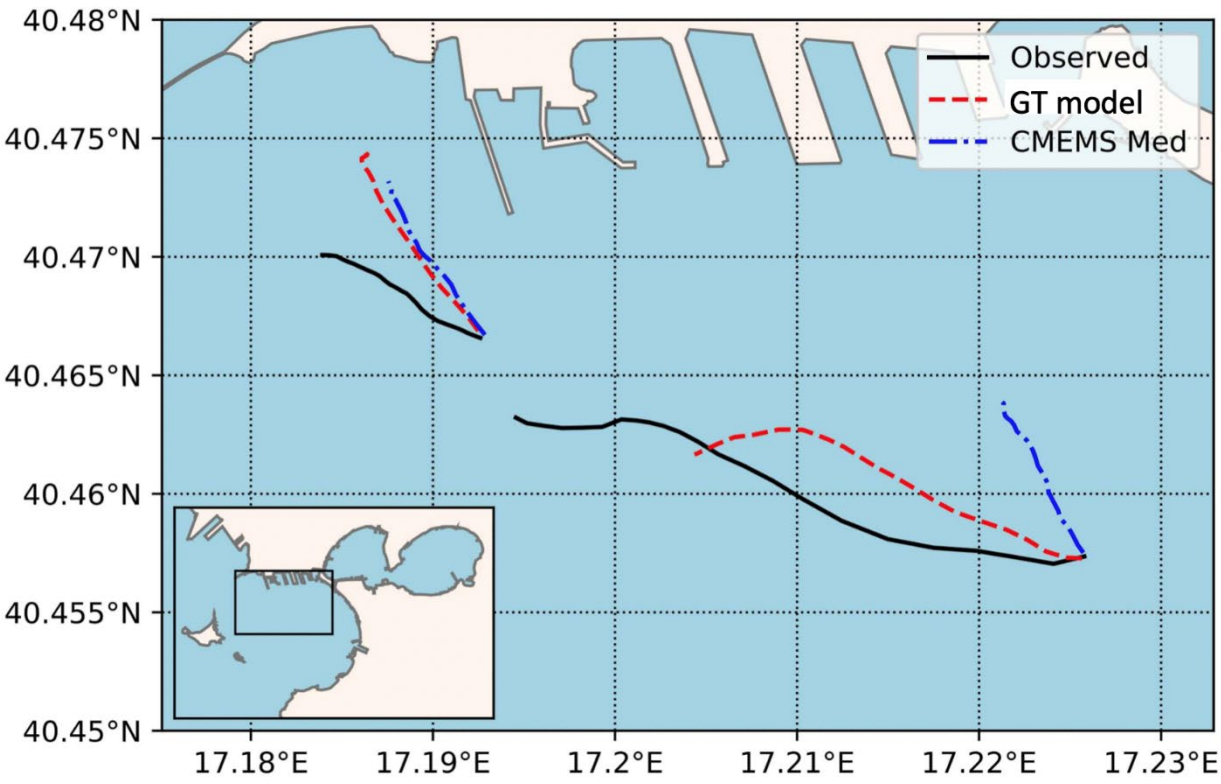

Figure 13. Mean drifter trajectories of the two drifter groups released in the Taranto Sea (black), and simulated drifter trajectories using the GT model(red) and CMEMS Med (blue).

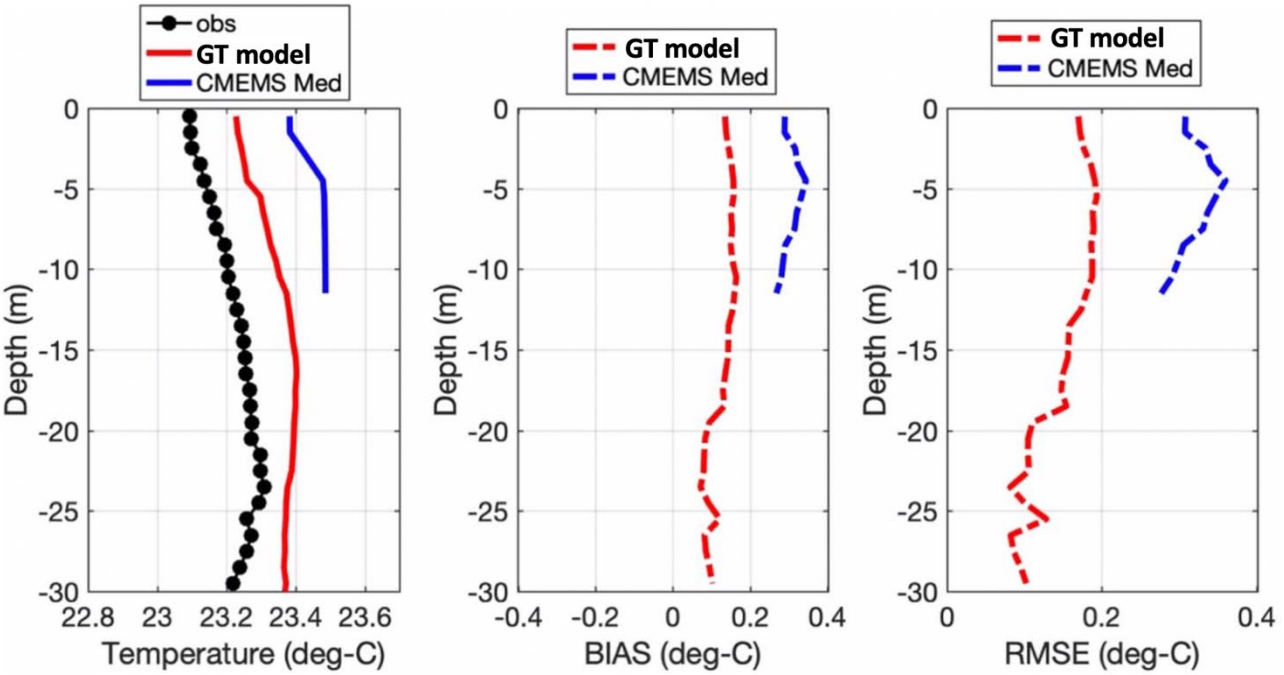

Figure 14. Comparisons between modelled (SURF-U and CMEMS Med) and observed CTD temperature profiles (left panel), with BIAS (middle panel) and RMSE (right panel). The observed temperature (black dotted line) is an average profile over the 31 CTD stations collected during the MREA14 survey in the Taranto Sea.

Barcelona

The OSPAC V1 operational simulation generates three-day forecasts of three-dimensional currents and other oceanographic variables, such as temperature, salinity, and sea level.

Figures 15, 16 and 17 show the ocean current fields (surface layer, near-bottom layer and different depths, respectively) on the Port domain and the highlighted Zoom of Barcelona's port and beaches on August 2, 2019. These results show a continuity sequence of the ocean currents field from the surface (higher values) to the near-bottom layer (smaller values and opposite ocean current direction than in the near-surface layers).

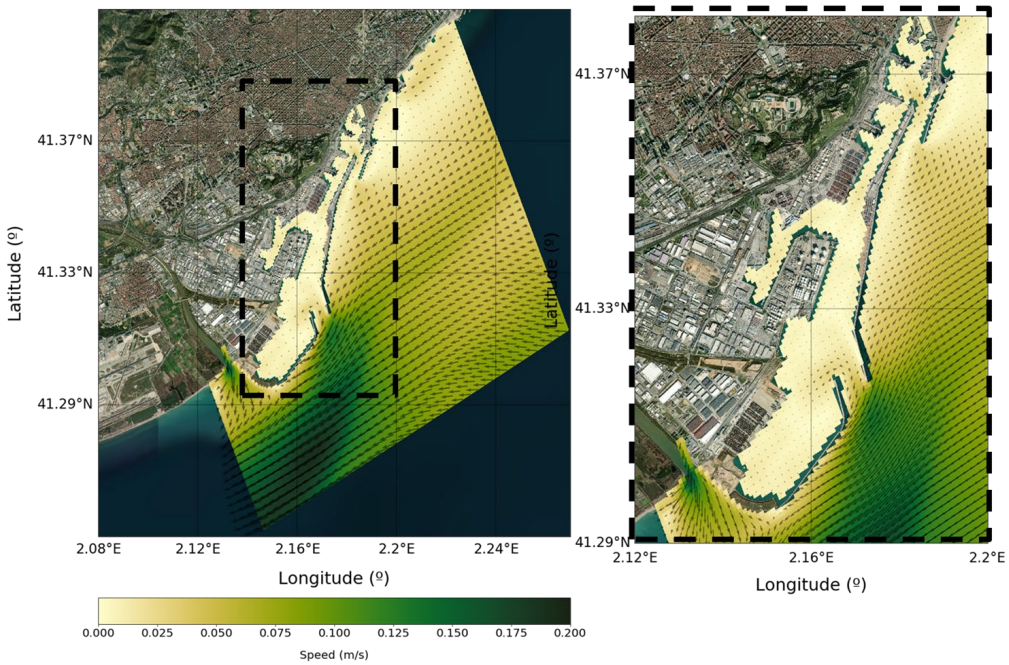

Figure 15. Magnitude of the velocity (colour scale) and direction of the surface current (vectors) on the Port domain (left panel) and on a highlighted Zoom of Barcelona's port and beaches (right panel) on August 2, 2019.

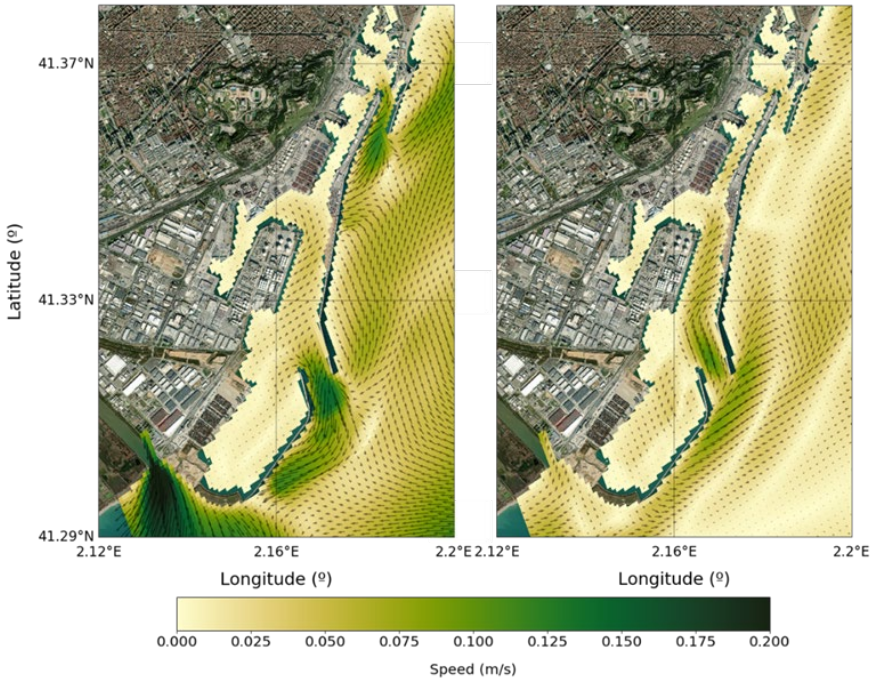

Figure 16. Magnitude of the velocity (colour scale) and direction of the surface current (vectors) in the surface layer (left panel) and near-bottom layer (right panel) on a highlighted Zoom of Barcelona's port and beaches (right panel) on August 2, 2019.

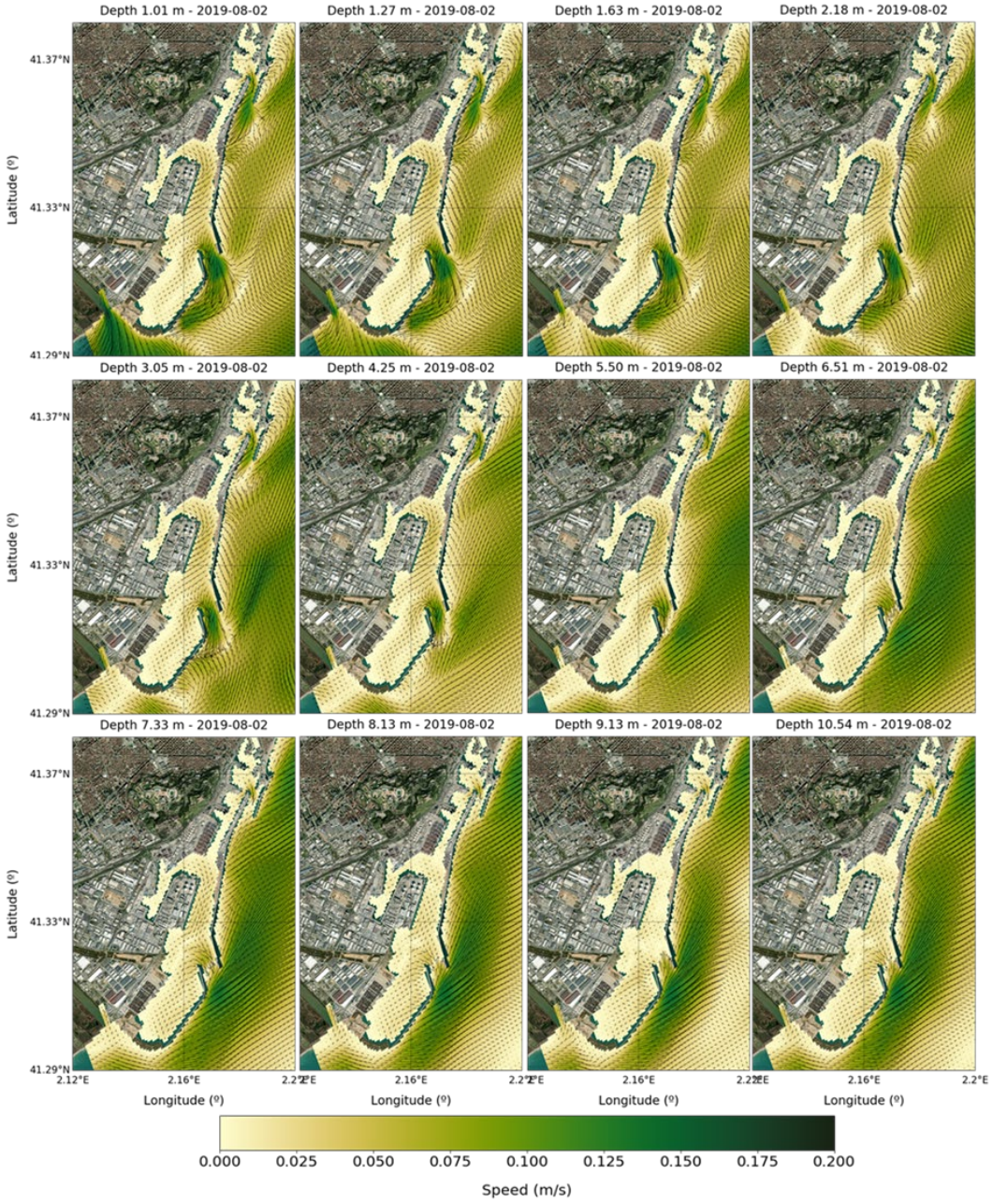

Figure 17. Magnitude of the velocity (colour scale) and direction of the surface current (vectors) at different depths on a highlighted Zoom of Barcelona's port and beaches on August 2, 2019.

Figure 18 shows surface and near-bottom temperature and salinity fields. In the same way as for ocean currents fields, these results show concordance: e.g., higher surface temperature values than near-bottom temperature values or smaller surface salinity values than near-bottom salinity values.

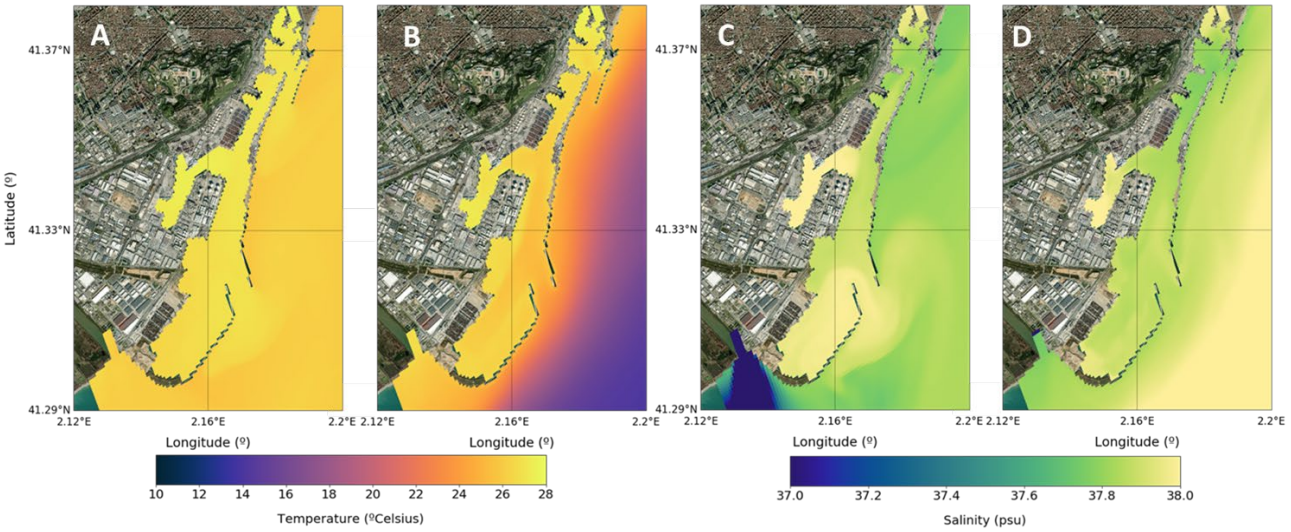

Figure 18. (A) Surface temperature, (B) near-bottom temperature, (C) surface salinity and (D) near-bottom salinity on a highlighted Zoom of Barcelona's port and beaches on August 2, 2019.

Product quality assessment is crucial for operational forecasting systems (Sotillo et al., 2019). Therefore, the model results have been validated with in situ observations from a field campaign in the Barcelona port during the summer of 2019. These validations are shown below.

Figure 19 shows the correlations (modelled data vs observations) drawn off at the blue cross point of the surface current speed and direction (A panel), the sea level (B panel) and the temperature (C panel) on a highlighted Zoom of Barcelona's port and beaches on August 2, 2019.

The correlation reaches values of 0.82 for the sea level or 0.94 for the temperature, while the correlation for surface current speed and direction shows values between 0.54-0.34, respectively. The surface current speed and direction correlations are expected to improve in the coupled version of OSPAC V2. In this way, the model provides results that will be used to develop new forecast capabilities, such as predicting erosion and flooding, simulating rip currents, tracking the floating debris, and knowing the flushing times.

Finally, we look ahead to the future of the development and maintenance of the operational prediction systems because their harmonisation and integration with the existing ocean knowledge will increase the availability of credible scientific evidence to inform industry, help to reduce the impact of human activities on the ocean and improve environmental management.

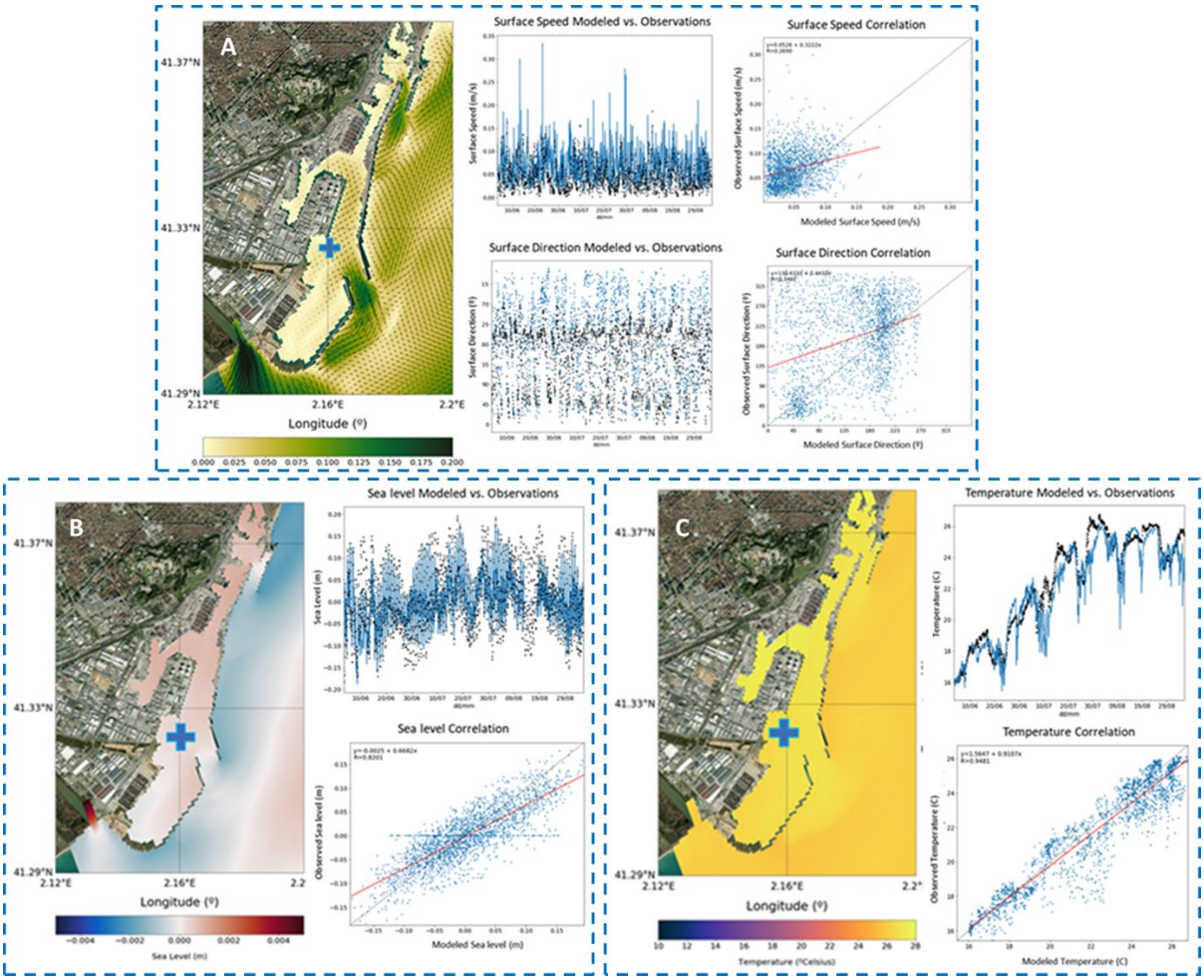

Figure 19. (A panel) Surface current speed (m/s), time series and correlations of surface speed and direction at the cross point drawn (modelled data vs observations). (B) Sea level (m), time series and correlation of sea level at the cross point drawn (modelled data vs observations. (C panel) Surface temperature (degree Celsius), time series and correlation of surface temperature at the cross point drawn (modelled data vs observations), on a highlighted Zoom of Barcelona's port and beaches on August 2, 2019.

5. Operational Forecasting Chains

Taranto

The operational chain built for the EUROSEA framework is capable every day to provide 3-days of forecasts with hourly frequency. The outputs have been delivered both in unstructured (native) format and regridded format to serve downstream services (e.g. tool for visualization) and applications. The ocean fields released on the daily basis are 3D currents, temperature and salinity, and sea level.

The operational forecasting methodology is based on the high-resolution model re-initialization every day, similar to the short-term limited-area atmospheric modelling practice (Mesinger et al., 1988). The re-initialization strategy allows exploiting the high-quality systematic fields of parent model Med CMEMS (provided by data assimilation), which supplies operational forecasting products in the framework of CMEMS service. This type of approach has been adopted by other forecasting systems downscaled from Med-CMEMS, as reported in Napolitano et al. (2016).

The daily forecast cycle for the model configuration is reported in Fig. 12a. With j as the current day, the initializing fields (taken from the Med-CMEMS simulation products) of forecast procedure are imposed at 12:00 of 3 days backward (j − 3) as the instantaneous fields. The forecasting run exploits the Med-CMEMS simulations (for j − 2 and j − 1) and the Med-CMEMS forecasts (for j +1, j +2 and j +3) at the lateral open boundary, while the surface boundary conditions run over the ECMWF analysis (j − 3, j − 2, j − 1) and forecasts (j + 1, j + 2, j + 3). The forecast is prepared and runs automatically. The operational chain is activated as soon as the atmospheric forcings are available. The technical procedures (Fig. 12b) through scripts and codes for computing the forecast fields can be summarized in the pre- processing of input data, model run and post-processing of the output model.

The main informatic procedures are based on workflow manager and python-based scripts.

Since the operational chain was designed with a scalability and reusability approach, the modules used there were relocated and further developed in order to manage the tasks required by the full operational cycle.

The main informatic aspects about the operational chains are:

- Managed workflow (python Luigi based[7])
    - No direct usage of cluster's scheduler
    - Already adopted in operational chains at CMCC
- No bash-based automations
    - Easier to maintain
    - Uncoupled function
    - Optimized I/O
- Consolidated production framework (e.g. Spotify)
- Pre-and-post processing intrinsically parallelized
    - Faster execution time for large dataset
    - Easy recover in case of failures
- Front-end included

The managed workflow vs. the flat automation design, allowed us to design and develop a more structured and modular system able to manage every aspect of the operational routines (unexpected situations included) and to serve as foundation for more complex and higher-level operations. The indirect usage of the cluster's scheduler makes it possible to choose amongst different running models, each fitting different cluster conditions and unexpected situations.

The bash automation was kept to a minimum, preferring the use of a general-purpose language to describe the operational tasks. This led to a more structured codebase, easier to maintain with a clear separation of concerns between modules.

The use of command-line based data manipulation tools has been eliminated in favor of the direct use of programmatic libraries that are at the foundation of the aforementioned commands. This allowed a more rationale usage of manipulation routines and a considerable reduction of disk usage for intermediate results storing.

[7] https://github.com/spotify/luigi

The workflow manager used to run operatively was Spotify's Luigi, a mature piece of software, already used in production by a large number of big IT industries. Luigi is a Free Open Source software too, which allow us to inspect its internals, make changes freely and contribute to the project.

The operational chain is constituted mainly by three large steps, each of which dealing with Preprocessing, model running/monitoring, Post processing. Being the pre and post processing are composed almost entirely by a large number of interpolations, there is a lot of room for parallelization. The way the tasks are designed, allowed us to exploit this intrinsic parallelization almost for free by splitting the large interpolations in blocks and by choosing a running model with different concurrent workers.

The first concern of the operational staff is to understand the state of the system in case of malfunctioning.

The Luigi's scheduler used in the operational chains integrates a web based front end showing in real time the status of every workflow running. In the schematic representation, each dot indicates a single task need to be accomplished in order to advance the workflow. The color of that dot denotes visually the state of the task, being: yellow when pending, green when done, blue when running, red when failed.

When hovering, each task shows the relevant details useful to precisely identify it and, in case of failure, details about the error are shown too.

The representation gives a consistent picture about the system state and simplifies the identification of problems.

The forecasting data are included in the OSPAC platform and also displayed at the website[8].

Barcelona

The daily operational chain built for the EUROSEA framework produces short-term (+3 Days) forecasts of hourly 3-D currents and other oceanographic variables, such as temperature, salinity, and sea level.

The system uses the ROMS model and consists of two nested regular grids with a spatial resolution of ~350 m and ~70 m for the coastal and harbour domains, respectively. In addition, the model is forced with very high-resolution atmospheric forcing (provided by the Spanish Meteorological Office AEMET). Finally, it is nested into the core Copernicus IBI regional solution (IBI_PHY hereafter) (see Figure 20).

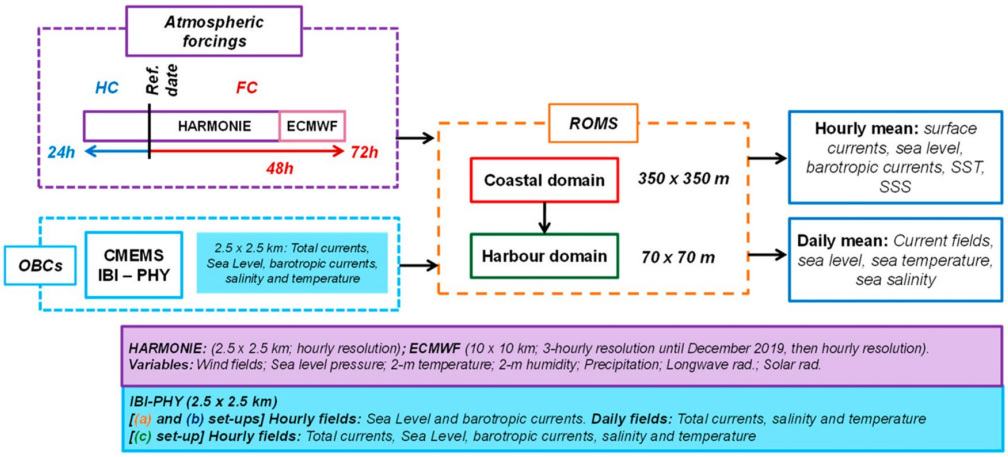

[8] https://taranto.cmcc.it/

Figure 20. Architecture of the EuroSea circulation forecast system for the Barcelona case. Operational scheme detailing the input data sources, including atmospheric forcing and the ocean solution imposed at the Open Boundary Conditions (OBCs), the numerical core (ROMS) with domain organization, and the delivered products (García-León, M et al., 2022).

The outputs have been delivered in NetCDF (native) and gridded format to serve downstream services (e.g. tool for visualization) and applications. The forecasting data are included in the OSPAC platform and also displayed at the website: https://www.puertos.es.

6. Conclusions

6.1. Taranto

A circulation modelling system based on the SHYFEM unstructured-grid model has been implemented for the entire Gulf of Taranto, with the specific focus and higher horizontal resolution (up to 20m) for the Taranto port and embayments. The variable mesh approach ensures continuity and mutual exchanges in seamless fashion among the different scales (sub-regional, coastal and port).

The connection with the regional scale of the Mediterranean Sea is done via downscaling approach based on CMEMS-Med products.

The coastal model has been validated over different sea state variables (sea level, currents and temperature) and against different observing data (satellite SST, CTD, tidegauges, drifters, ADCP), showing a good agreement.

The comparison with CMEMS-Med model shows the added value of the coastal model and the augmentation of the realism of the ocean hydrodynamics at coastal scale thanks to the downscaling strategy (higher spatial resolution including geometric features of the coastal areas, specific input dataset, parametrizations and processes for coastal scale).

Future works will be oriented (i) to a deeper assessment of the wave contribution to the circulation including different drivers (i.e. air-sea momentum transfer and turbulence induced by waves); (ii) to the validation of the operational forecasting products; (iii) to explore the possibility of ensemble coastal downscaling from the MedEns system developed in WP4.

6.2. Barcelona

In this deliverable, we've compared the results of grid downscaling for the Calatan Coast. In addition, the OSPAC V1 operational system (ROMS ocean model) has been implemented in Barcelona's port and coastal waters using initial and boundary conditions from the open and free-access general circulation model systems available in the Copernicus Marine Environment Monitoring Service (CMEMS, Le Traon et al., 2019) online catalogue.

We've investigated how increased model spatial resolution improves hydrodynamic variables forecasts. We've also validated these results with field campaign data on summer'19 founding good agreements between model results and measured data.

Future efforts are planned to improve the accuracy of the hydrodynamic results using CMEMS products in several aspects already addressed in the present deliverable. While the OSPAC V1 operational system has already been tested and validated, OSPAC V2 will evolve towards an operational model application and is

expected to positively impact a more accurate representation of coastal and local processes. At the same time, other factors that could be improved but still deserve further analysis are refined mixing schemes, which could better represent water masses, and the air-sea and land-sea interactions (i.e., weather forcings and fluvial forcing), from which coastal circulation could be better described.

7. References

7.1. Taranto

Artegiani, A., Bregant, D., Paschini, E., Pinardi, N, Raicich, F., Russo, A., (1997a). The Adriatic Sea general circulation. Part I: Air-sea interactions and water mass structure, *J. Phys. Oceanogr.*, 27, 1492–1514.

Artegiani, A., Bregant, D., Paschini, E., Pinardi, N., Raicich, F., Russo, A. (1997b) The Adriatic Sea general circulation. Part II: Baro- clinic circulation structure, *J. Phys. Oceanogr.*, 27, 1515–1532.

Bellafiore, D., Umgiesser, G., 2010. Hydrodynamic coastal processes in the north Adriatic investigated with a 3D finite element model, *Ocean Dynam.*, 60, 255–273.

Bignami, F., Sciarra, R., Carniel, S., Santoleri, R., 2007. Variability of Adriatic Sea coastal turbid waters from SeaWiFS imagery, *J. Geophys. Res.*, 112, 3–10.

Burchard, H., Bolding, K., Villarreal, M.R., 1999. GOTM—a general ocean turbulence model. Theory, applications and test cases. Technical Report EUR 18745 EN, European Commission.

Caroppo, C., Giordano, L., Rubino, F., Palmieri, N., Bellio, G., Bisci, A., Petrocelli, A., Sclafani, P., Hopkins, T., Marsella, E., 2011. Sustainable management of the coastal environments in the framework of the SPICOSA Project: the study case of the Mar Piccolo in Taranto (Ionian, Mediterranean Sea). In *Marine Research* at CNR:928–942

Cerruti, A., 1948. Le sorgenti sottomarine (Citri) del Mar Grande e nel Mar Piccolo di Taranto. *Annali Istituto Superiore Navale*, Napoli 7:171–196 (in Italian)

Ciancia, E., Coviello, I., Di Polito, C., Lacava, T., Pergola, N., Satriano, V., Tramutoli, V., 2018. Investigating the chlorophyll-a variability in the Gulf of Taranto (North-western Ionian Sea) by a multi-temporal analysis of MODIS-Aqua Level 3/Level 2 data, *Continental Shelf Research*, 155, 34-44.

Cressman, G.P., 1959. An operational objective analysis scheme, Mon. Weather Rev., 87, 367–374.

Cushman-Roisin, B., Gacic, M., Poulain, P., Artegiani, A., 2001. Physical Oceanography of the Adriatic Sea: Past, Present, and Future, Kluwer Acad., Dordrecht, the Netherlands, 304 pp.

De Pascalis, F., Petrizzo, A., Ghezzo, M., Lorenzetti, G., Manfé, G., Alabiso, G., Zaggia, L., 2016. Estuarine circulation in the Taranto Seas, Integrated environmental characterization of the contaminated marine coastal area of Taranto, Ionian Sea (south- ern Italy), the RITMARE Project, *Environ. Sci. Pollut. R.*, 23, 12515–12534.

De Serio, F., Mossa, M. (2015). Analysis of mean velocity and turbulence measurements with ADCPs, *Adv. Water Res.*, 81, 172–185.

Dobricic, S., Pinardi, N., 2008. An oceanographic three-dimensional variational data assimilation scheme, *Ocean Model.*, 22, 89–105.

Egbert, G., Erofeeva, S., 2002. Efficient inverse modeling of barotropic ocean tides, J. Atmos. Ocean. Tech., 19, 183–204.

Ferrarin, C., Roland, A., Bajo, M., Umgiesser, G., Cucco, A., Davolio, S., Buzzi, A., Malguzzi, P., Drofa, O., 2013. Tide-surge-wave modelling and forecasting in the Mediterranean Sea with focus on the Italian coast, *Ocean Model.*, 61, 38–48.

Ferrarin, C., Bajo, M., Bellafiore, D., Cucco, A., De Pascalis, F., Ghezzo, M., Umgiesser, G., 2014. Toward homogenization of Mediterranean lagoons and their loss of hydrodiversity. *Geophys Res Lett* 41(16):5935–5941.

Ferrarin C, Maicu F, Umgiesser G., 2017. The effect of lagoons on Adriatic Sea tidal dynamics. *Ocean Model*., 119:57–71.

Federico, I., Pinardi, N., Coppini, G., Oddo, P., Lecci, R., Mossa, M., 2017. Coastal ocean forecasting with an unstructured grid model in the Southern Adriatic and Northern Ionian seas, *Nat. Hazards Earth Syst. Sci.*, 17, 45–59.

Grauel, A. L., Bernasconi, S. M., 2010. Core-top calibration of δ18O and δ13O of G. ruber (white) and U. mediterranea along the southern Adriatic coast of Italy, *Mar. Micropaleontol*., 77, 175– 186.

Hellermann, S., Rosenstein, M., 1983. Normal wind stress over the world ocean with error estimates, *J. Phys. Oceanogr.*, 13, 1093–1104.

Kara, B. A., Wallcraft, A. J., Hurlburt, H. E., 2007. A Correction for Land Contamination of Atmospheric Variables near Land–Sea Boundaries, *J. Phys. Oceanogr.*, 37, 803–818.

Madec, G. (2008). NEMO ocean engine, Note du Pole de modelisation, Institut Pierre-Simon Laplace (IPSL), France, 27, 1288–1619.

Milligan, T.G., Cattaneo, A., 2007. Sediment dynamics in the western Adriatic Sea: From transport to stratigraphy, *Cont. Shelf Res.*, 27, 287–295.

Oddo, P., Guarnieri, A., 2011. A study of the hydrographic conditions in the Adriatic Sea from numerical modelling and direct observations (2000–2008), Ocean Sci., 7, 549–567.

Pettenuzzo, D., Large, W. G., and Pinardi, N., 2010. On the corrections of ERA40 surface flux products consistent with the Mediterranean heat and water budgets and the connection between basin surface total heat flux and NAO, *J. Geophys. Res.*, 115, C06022

Pinardi, N., Lyubartsev, V., Cardellicchio, N., Caporale, C., Ciliberti, S., Coppini, G., De Pascalis, F., Dialti, L., Federico, I., Fil- ippone, M., Grandi, A., Guideri, M., Lecci, R., Lamberti, L., Lorenzetti, G., Lusiani, P., Macripo, C. D., Maicu, F., Mossa, M., Tartarini, D., Trotta, F., Umgiesser, G., Zaggia, L., 2016. Marine Rapid Environmental Assessment in the Gulf of Taranto: a multiscale approach, *Nat. Hazards Earth Syst. Sci.*, 16, 2623–2639.

Poulain, P. M., 2001. Adriatic Sea surface circulation as derived from drifter data between 1990 and 1999, *J. Mar. Syst.* 29, 3–32.

Scroccaro, I., Matarrese, R., Umgiesser, G., 2004, Application of a finite element model to the Taranto Sea. *Chem. Ecol.*, 20:205–224, supplement 1.

Sellschopp, J., Alvarez, A., 2003. Dense low-salinity outflow from the Adriatic Sea under mild (2001) and strong (1999) winter conditions, *J. Geophys. Res.*, 108, 8104.

Spizzico, M., Tinelli, R., 1986. Hydrogeology of Galese spring, Mar Piccolo of Taranto (S. Italy). In: *Proceedings 9th Salt Water Intrusion Meeting Delft, Water Management Group*, Delft University of Technology, pp 85–97

Stefanon, A., Cotecchia, F., 1969. Prime notizie sulle caratteristiche di efflusso e sulle modalità di investigazione delle sorgenti sub-acquee ai fini di una loro captazione. *Quaderni de La Ricerca Scientifica, Istituto di Ricerca sulle Acque* 58(Rapporto n. 2): 165–195 (in Italian)

Turchetto, M., Boldrin, A., Langone, L., Miserocchi, S., Tesi, T., Foglini, F., 2007. Particle transport in the Bari Canyon (southern Adriatic Sea), *Mar. Geol.*, 246, 231–247.

Umgiesser, G., Canu, D. M., Cucco, A., Solidoro, C., 2004. A finite element model for the Venice lagoon: Development, set up, calibration and validation, *J. Marine Syst.*, 51, 123–145.

Umgiesser, G., Ferrarin, C., Cucco, A., De Pascalis, F., Bellafiore, D., Ghezzo, M., Bajo, M., 2014. Comparative hydrodynamics of 10 Mediterranean lagoons by means of numerical modeling, *J. Geophys. Res.-Oceans*, 119, 2212–2226.

Verri, G., Pinardi, N., Oddo, P. et al., 2018. River runoff influences on the Central Mediterranean overturning circulation. Clim. Dyn., 50, 1675–1703. https://doi.org/10.1007/s00382-017-3715-9

7.2. Barcelona

Arnau, P. A., 2000. Aspectos de la variabilidad de mesoescala de la circulación marina en la plataforma continental catalana (Ph.D. thesis). Universitat Poli- tecnica de Catalunya.

Bolaños, R., Jordà, G., Cateura, J., Lopez, J., Puigdefabregas, J., Gomez, J., Espino, M., 2009. The XIOM: 20 years of a regional coastal observatory in the Spanish Catalan coast. J. Mar. Syst.77,237–260.

Booij, N., Ris, R.C., Holthuijsen, L.H., 1999. A third-generation wave model for coastal regions. Part I: Model description and validation. Journal of Geophysical Research 104 (C4), 7649–7666.

Buongiorno Nardelli B., Tronconi, C., Pisano, A., Santoleri, R., 2013. High and Ultra-High resolution processing of satellite Sea Surface Temperature data over Southern European Seas in the framework of MyOcean project, Rem. Sens. Env., 129, 1-16, doi:10.1016/j.rse.2012.10.012.

Carter GS, Merrifield MA. 2007. Open boundary conditions for regional tidal simulations. Ocean Model. 18:194–209. doi:10.1016/j.ocemod.2007.04.003.

García-León, M.; Sotillo, M.G.; Mestres, M.; Espino, M.; Fanjul, E.Á. Improving Operational Ocean Models for the Spanish Port Authorities: Assessment of the SAMOA Coastal Forecasting Service Upgrades. J. Mar. Sci. Eng. 2022, 10, 149. https://doi.org/10.3390/jmse10020149

Haidvogel, D. B. , Arango, H.G., Budgell, W. P., Cornuelle, B. D., Curchitser, E., Di Lorenzo, E., Fennel, K., Geyer, W. R., Hermann, A. J., Lanerolle, L., Levin, J., McWilliams, J. C., Miller, A. J., Moore, A. M., Powell, T.

M., Shchepetkin, A. F., Sherwood, C. R., Signell, R. P., Warner, J. C., Wilkin, J. (2008). Ocean forecasting in terrain-following coordinates: Formulation and skill assessment of the Regional Ocean Modeling System, Journal of Computational Physics. 227, 3595-3624.

Le Traon, P. Y., Reppucci, A., Reppucci, A., Fanjul, E. A., Aouf, L., Behrens, A., et al. (2019). From Observation to Information and Users: the Copernicus Marine Service Perspective. Front. Mar. Sci. 6:234. doi: 10.3389/fmars.2019.00234.

Liste ,M., Mestres, M., Espino, M., Sanchez-Arcilla, A., García-León, M., Sotillo, M., and Alvarez-Fanjul, E. (2021). High-Resolution 3D Forecasting System for Barcelona's Beaches and Coastal Waters. EGU General Assembly. 19-30 April 2020. Vienna, Austria.

Mendoza, E.T., Jiménez, J.A., Mateo, J., 2011. A coastal storms intensity scale for the Catalan Sea (NW Mediterranean). Natural Hazards Earth Syst. Sci. 11, 2453–2462.

Mestres M, Grifoll M, Sánchez-Arcilla A. 2016. Analysis of current intensification in the Northwest Mediterranean shelf. Cont Shelf Res. 114:29–40. ISSN 0278-4343, doi:10.1016/j.csr.2015.12.011.

Pallares, E., Sánchez-Arcilla, A., and Espino, M., 2014. Wave energy balance in wave models (SWAN) for semi-enclosed domains - Application to the Catalan coast. Continental Shel fResearch 87(2014), 41–53. http://dx.doi.org/10.1016/j.csr.2014.03.008.

Poulain, P.-M., Bussani, A., Gerin, R., Jungwirth, R., Mauri, E., Menna, M., Notar-Stefano, G., 2013. Mediterranean surface currents measured with drifters: from basin to subinertial scales. Oceanography 26(1), 38–47. http://dx.doi.org/10.5670/oceanog.2013.03.

Sánchez-Arcilla, A. and Simpson, J., 2002.The narrow shelf concept: couplings and fluxes.Cont. Shelf Res. 22(2), 153–172.

Sánchez-Arcilla, A., González-Marco, D., Bolaños, R., 2008. A review of wave climate and prediction along the Spanish Mediterranean coast. Natural Hazards Earth Syst. Sci. 8, 1217–1228.

Shchepetkin, A. F., McWilliams, J.C. (2005). The Regional Oceanic Modeling System: A split-explicit, free-surface, topography-following coordinate oceanic model. Ocean Modeling 9, 347–404 doi:10.1016/j.ocemod.2004.08.002.

Shchepetkin, A. F., McWilliams, J. C. (2009). Correction and commentary for “Ocean forecasting in terrain-following coordinates: Formulation and skill assessment of the regional ocean modeling system” by Haidvogel et al., J. Comp. Phys. 227, pp. 3595–3624.”. Journal of Computational Physics. 228, 8985-9000.

Sotillo, MG., P. Cerralbo, P. Lorente, M. Grifoll, M. Espino, A. Sanchez- Arcilla & E. Álvarez-Fanjul (2019): Coastal ocean forecasting in Spanish ports: the SAMOA operational service, Journal of Operational Oceanography, DOI: 10.1080/1755876X.2019.1606765

Sotillo MG, Cailleau S, Lorente P, Levier B, Aznar R, Reffray G, AmoBaladrón A, Chanut J, Benkiran M, Alvarez-Fanjul E. 2015. The MyOcean IBI ocean forecast and reanalysis systems: operational products and roadmap to the future Copernicus service. J Oper Oceanogr. 8(1):63–79. doi:10. 1080/1755876X.2015.1014663.

Tsimplis, M.N., Proctor, R., Flather, R.A., 1995.A two-dimensional tidal model for the Mediterranean Sea. J. Geophys. Res. 100 (C8), 16223–16239. http://dx.doi.org/10.1029/95JC01671.

Warner, J.C., Armstrong, B., He, R., and Zambon, J. (2010). Development of a Coupled Ocean-Atmosphere-Wave-Sediment Transport (COAWST) Modeling System, Ocean Modelling, 35, 230-244. (http://woodshole.er.usgs.gov/project-pages/cccp/public/COAWST.htm).

Warner JC, Sherwood CR, Arango HG, Signell RP. 2005. Performance of four turbulence closure models implemented using a generic length scale method. Ocean Model. 8(1):81–113.